Regulation of cell proliferation by ERK and signal-dependent nuclear translocation of ERK is dependent on Tm5NM1-containing actin filaments

Galina Schevzov[a,*], Anthony J. Kee[b,*], Bin Wang[a,*], Vanessa B. Sequeira[a], Jeff Hook[a], Jason D. Coombes[a,c], Christine A. Lucas[b], Justine R. Stehn[a], Elizabeth A. Musgrove[d,†], Alexandra Cretu[e], Richard Assoian[e], Thomas Fath[f], Tamar Hanoch[g], Rony Seger[g], Irina Pleines[h], Benjamin T. Kile[h], Edna C. Hardeman[b,‡], and Peter W. Gunning[a,‡]

[a]Oncology Research Unit, School of Medical Sciences, [b]Cellular and Genetic Medicine Unit, and [f]Neurodegeneration and Repair Laboratory, School of Medical Sciences, University of New South Wales, Australia, Sydney, NSW 2052, Australia; [c]Sydney Medical School, University of Sydney, Sydney, NSW 2006, Australia; [d]Kinghorn Cancer Centre, Cancer Research Program, Garvan Institute of Medical Research, Darlinghurst, Sydney, NSW 2010, Australia; [e]Department of Pharmacology, Perelman School of Medicine, University of Pennsylvania, Philadelphia, PA 19104-6160; [g]Department of Biological Regulation, Weizmann Institute of Science, Rehovot 76100, Israel; [h]Cancer and Hematology Division, Walter and Eliza Hall Institute of Medical Research, Parkville, VIC 3052, Australia

ABSTRACT **ERK-regulated cell proliferation requires multiple phosphorylation events catalyzed first by MEK and then by casein kinase 2 (CK2), followed by interaction with importin7 and subsequent nuclear translocation of pERK. We report that genetic manipulation of a core component of the actin filaments of cancer cells, the tropomyosin Tm5NM1, regulates the proliferation of normal cells both in vitro and in vivo. Mouse embryo fibroblasts (MEFs) lacking Tm5NM1, which have reduced proliferative capacity, are insensitive to inhibition of ERK by peptide and small-molecule inhibitors, indicating that ERK is unable to regulate proliferation of these knockout (KO) cells. Treatment of wild-type MEFs with a CK2 inhibitor to block phosphorylation of the nuclear translocation signal in pERK resulted in greatly decreased cell proliferation and a significant reduction in the nuclear translocation of pERK. In contrast, Tm5NM1 KO MEFs, which show reduced nuclear translocation of pERK, were unaffected by inhibition of CK2. This suggested that it is nuclear translocation of CK2-phosphorylated pERK that regulates cell proliferation and this capacity is absent in Tm5NM1 KO cells. Proximity ligation assays confirmed a growth factor–stimulated interaction of pERK with Tm5NM1 and that the interaction of pERK with importin7 is greatly reduced in the Tm5NM1 KO cells.**

Monitoring Editor
Valerie Marie Weaver
University of California, San Francisco

Received: Oct 16, 2014
Revised: May 5, 2015
Accepted: May 7, 2015

This article was published online ahead of print in MBoC in Press (http://www.molbiolcell.org/cgi/doi/10.1091/mbc.E14-10-1453) on May 13, 2015.

*These authors contributed equally.

†Present address: Wolfson Wohl Cancer Research Centre, University of Glasgow Garscube Estate, Bearsden, Glasgow G61 1BD, United Kingdom.

‡The laboratories of these authors contributed equally.

G.S., P.W.G., A.J.K., and V.B.S. wrote the manuscript with input from E.C.H. G.S. and A.J.K. designed, performed, and analyzed experiments. J.H., J.D.C., B.W., C.A.L., A.C., T.H., and I.P. performed and analyzed experiments. R.A., T.F., R.S., J.R.S., V.B.S., and B.T.K. supervised research. E.A.M. provided initial intellectual input to the study and critical editing of the manuscript. E.C.H. and P.W.G. directed the study.

Conflict of interest: P.G. is a director and J.R.S. is an employee of Novogen, a company that is developing anti-Tm5NM1 drugs as anticancer therapeutics.

Address correspondence to: Peter W. Gunning (p.gunning@unsw.edu.au).

Abbreviations used: CK2, casein kinase 2; ERK1/2, extracellular signal-regulated kinases 1/2; Imp7, importin 7; JNK, c-Jun-N-terminal kinase; KO, knockout; MAPK, mitogen-activated protein kinase; MEK, MAP/ERK kinase; NTS, nuclear translocation sequence; PI3K, phosphatidylinositol 3-kinase; PLA, proximity ligation assay; qRT-PCR, quantitative real-time-PCR; SPS, Ser-244/Pro-245/Ser-246; TEY, Thr-Glu-Tyr motif; TG, transgenic; Tm, tropomyosin; Tm5NM1, tropomyosin isoform 5 nonmuscle 1; WAT, white adipose tissue; WT, wild type.

Supplemental Material can be found at:
http://www.molbiolcell.org/content/suppl/2015/05/11/mbc.E14-10-1453v1.DC1.html

INTRODUCTION

Constitutive activation of the mitogen-activated protein kinase (MAPK) signaling pathways is the primary driver of cell proliferation in most cancers (Roberts and Der, 2007). These pathways consist of distinct tiers of conserved protein serine/threonine kinases that define each pathway and include the well-characterized extracellular signal-regulated kinases 1/2 (ERK1/2, termed here ERK), c-Jun-N-terminal kinase (JNK), p38 MAPK (Roskoski, 2012), and ERK5 (Nithianandarajah-Jones *et al.*, 2012). Activation of each MAPK requires dual phosphorylation of specific residues within the activation loop. For example, ERK is initially phosphorylated by MAPK/ERK kinase (MEK) on the Thr-Glu-Tyr (TEY) motif (Seger and Krebs, 1995), with subsequent phosphorylation on the Ser-244/Pro-245/Ser-246 (SPS) nuclear translocation sequence (NTS) mainly by casein kinase 2 (CK2) to generate pSPS-pERK (Chuderland *et al.*, 2008; Plotnikov *et al.*, 2011). These events lead to the nuclear translocation of ERK by the interaction of the phosphorylated NTS with the nuclear shuttling protein importin7 (Imp7) (Chuderland *et al.*, 2008). This cascade of well-defined events is essential for ERK-induced cell cycle regulation (Weber *et al.*, 1997; Schwartz and Assoian, 2001).

The actin cytoskeleton is a key regulator of numerous cellular functions, including proliferation and entry into the S phase of the cell cycle (Bohmer *et al.*, 1996; Huang *et al.*, 1998; Huang and Ingber, 2002; Reshetnikova *et al.*, 2000); however, the mechanism by which the cytoskeleton regulates cell proliferation has not been well defined. There is increasing evidence of interaction between actin filaments and components of the MAPK signal transduction pathways, with early reports suggesting a dependence on actin filaments for MAPK-regulated cell proliferation (Leinweber *et al.*, 1999; Aplin *et al.*, 2001; McNicol *et al.*, 2001; Harrison *et al.*, 2004; Smith *et al.*, 2004; Jongstra-Bilen and Jongstra, 2006; Ren *et al.*, 2007; White *et al.*, 2009). Several reports detected ERK in the Triton X-100–insoluble fraction, which is consistent with an association with the actin cytoskeleton (Atten *et al.*, 1998; Leinweber *et al.*, 1999; Schrick *et al.*, 2007). Morgan and coworkers showed costaining of ERK with actin stress fibers and found that release of ERK from stress fibers might be required for activation of ERK (Vetterkind *et al.*, 2013). Thus the actin cytoskeleton has been seen as a cytoplasmic anchor for ERK and potential inhibitor of ERK function.

The weakness with this view of the role of the actin cytoskeleton is the intrinsic assumption that the actin filaments as visualized by phalloidin staining or fractionated by Triton X-100 solubility are compositionally generic. Instead, it has become increasingly clear that this is not true (Michelot and Drubin, 2011). The two cytoskeletal actin isoforms are spatially segregated and functionally distinct (Schevzov *et al.*, 1992; Dugina *et al.*, 2009; Bunnell and Ervasti, 2011). In addition, tropomyosin (Tm) is an integral component of most actin filaments in all metazoan cells (Gunning *et al.*, 2008). The specific Tm incorporated into actin filaments, at least in yeast, is specified by the formin used to build the actin filament (Johnson *et al.*, 2014). The functional diversity of actin filament populations is controlled, at least in part, by the Tm component of actin filaments (Gunning *et al.*, 2008; O'Neill *et al.*, 2008). It is therefore possible that if the actin cytoskeleton is involved in cell proliferation, it will be mediated by a specific population of actin filaments containing a specific Tm.

Transformation of cells is accompanied by profound changes in the Tm isoform composition of their actin cytoskeleton (Hendricks and Weintraub, 1984; Lin *et al.*, 1985). There are only two Tm isoforms consistently retained by all human cancer cells thus far examined, tropomyosin isoform 5 nonmuscle 1 (Tm5NM1) and Tm4 (Stehn *et al.*, 2006, 2013). We previously reported that Tm5NM1 is essential for embryonic stem cell proliferation (Hook *et al.*, 2011) and cancer cell survival (Stehn *et al.*, 2013) and that expression of this isoform increases after release of NIH3T3 cells from quiescence back into the cell cycle (Percival *et al.*, 2000; Stehn *et al.*, 2013). These results point to Tm5NM1-containing actin filaments in actin-mediated cell proliferation. We used genetically manipulated mice and cells derived from them to test the role of Tm5NM1 in regulating cell proliferation in vivo and in vitro. Tm5NM1 was found to be required for the regulation of cell proliferation by ERK and the signal-dependent nuclear translocation of ERK.

RESULTS

Tm5NM1 promotes cell proliferation in vitro

To determine whether Tm5NM1 has a role in cell proliferation, we analyzed primary MEFs isolated from wild-type (WT) and Tm5NM1 knockout (KO) and transgenic (TG) mice. Tm5NM1 TG MEFs express twofold higher levels of Tm5NM1 than WT MEFs, whereas Tm5NM1 expression is undetectable in the KO MEFs (Figure 1, A and B). In cell proliferation assays using synchronized cells, we found that TG MEFs had an enhanced cell proliferation, whereas KO MEFs displayed reduced cell proliferation (Figure 1C). The observed defect in cell proliferation was also evident at lower (2.5%) and higher (15%) serum levels (Supplemental Figure S1) We observed a similar reduced proliferation rate in Tm5NM1 KO MEFs harvested from mice of a different genetic background, indicating that the decrease in proliferation is robust (Supplemental Figure S2, A and B). Restoration of Tm5NM1 expression by mating KO and TG mice rescued the phenotypes, and MEFs isolated from these mice have a proliferation rate similar to MEFs harvested from WT mice (Figure 1, D–F). Flow cytometry analysis of the Tm5NM1 KO MEFs showed no significant changes in the percentage of cells detected at different phases of the cell cycle compared with WT MEFs (Supplemental Figure S3A). This is an expected outcome. We predict that the observed proliferation defect is likely due to a change in G1. Owing to the slow doubling time of these cells (36–48 h; unpublished data) together with the observation that ~60% of the cells are in G1 (Supplemental Figure S3A), it is unlikely that a statistically significant change in the fraction of cells in G1 would be detected. In addition, knocking out or overexpressing Tm5NM1 does not result in compensation by other Tm isoforms (Supplemental Figure S3, B–D).

To confirm that the decrease in proliferation was due to an isoform-specific effect, we examined the effect of the loss of Tm4, another low–molecular weight Tm isoform consistently expressed in both normal and cancer cells (Stehn *et al.*, 2013), on cell proliferation. Functional knockout of Tm4 in *Tpm4*$^{Plt53/Plt53}$ MEFs had no effect on proliferation relative to WT MEFs (Figure 1, G–I). Of importance, depletion of Tm4 protein had no effect on the levels of Tm5NM1 (Figure 1G). Collectively these data indicate that the effect on proliferation observed in the KO and TG MEFs is specifically a consequence of altered Tm5NM1 expression levels.

It is well established that cell proliferation is influenced by cell–substratum interactions, and the actin cytoskeleton is implicated in this biological response (Assoian and Klein, 2008). In particular, cells display a graded proliferative response to changes in substratum compliance (Klein *et al.*, 2009). In this study, the reduced proliferation rate of Tm5NM1 KO MEFs was unrelated to their ability to respond to changes in substratum compliance (Supplemental Figure S3E).

Tm5NM1 promotes cell proliferation in vivo

To determine whether perturbation of Tm5NM1 levels in vivo has any effect on cell proliferation, we analyzed tissues from Tm5NM1

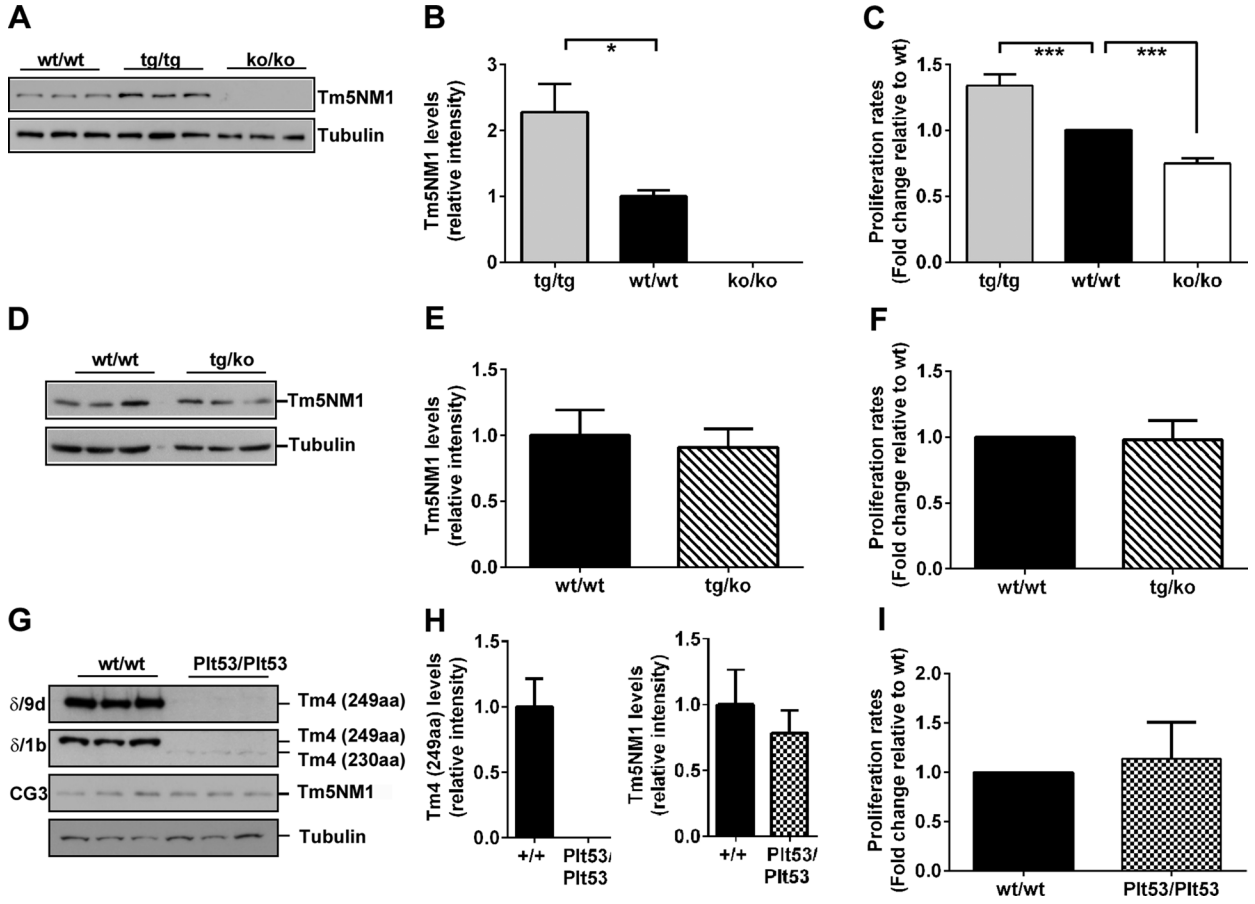

FIGURE 1: Tm5NM1 regulates cell proliferation in vitro. (A) Representative Western blot of WT (wt/wt), Tm5NM1 TG (tg/tg), and KO (ko/ko) MEFs probed with γ/9d (Tm5NM1) and α-tubulin (to evaluate protein loading) antibodies. (B) Quantification of Tm5NM1 levels in A; WT was set at 1. *$p < 0.05$. (C) MEFs were growth arrested by serum deprivation and allowed to reenter the cell cycle with the addition of 10% (vol/vol) FBS, and cells were counted. Proliferation rate was determined from the slope of the linear regression curves and plotted as a fold change relative to WT MEFs (set at 1). $n = 4$; ***$p < 0.001$. (D) Representative Western blot of WT (wt/wt) and Tm5NM1 TGxKO (tg/ko) MEFs probed with γ/9d (Tm5NM1) and α-tubulin (to evaluate protein loading). (E) Quantification of Tm5NM1 levels in D; WT was set at 1. (F) Proliferation rates of WT and Tm5NM1 TG/KO MEFs determined as described in C ($n = 3$); WT was set at 1. (G) Representative Western blots of WT (wt/wt) and Tm4 functional KO (Plt53/Plt53) MEFs probed with δ/9d and δ/1b antibodies (which detect full-length and truncated Tm4 protein, respectively), CG3 (Tm5NM1), and α-tubulin (to evaluate protein loading). (H) Quantification of Tm4 and Tm5NM1 levels in G; WT was set at 1. (I) Proliferation rates of WT (wt/wt) and Tm4 functional KO (Plt53/Plt53) MEFs determined as described in C ($n = 3$); WT was set at 1.

KO and TG mice described previously (Bryce *et al.*, 2003; Kee *et al.*, 2004; Vlahovich *et al.*, 2009). Most striking was the variation in weight of white adipose tissue (WAT) depots between these mouse lines (Figure 2, A and B). The weight of both abdominal (epididymal and retroperitoneal) and subcutaneous (inguinal) WAT depots as a percentage of body weight was increased in adult (3-mo-old) TG mice and reduced in KO mice compared with WT controls (Figure 2, A and B). Similar changes occurred in brain and kidney mass, with a significant decrease observed in KO mice and an increase in TG mice (Figure 2, C and D). Total body fat mass was higher in the TG mice and reduced in the KO mice (Supplemental Figure S4A). However, the body weights of TG and KO mice were similar to that of their WT controls (Supplemental Figure S4B) since there was a significant decrease and increase in lean body mass in TG and KO mice, respectively, as determined by dual x-ray absorptiometry (Supplemental Figure S4A).

WAT mass was unchanged in a TG mouse overexpressing a different Tm isoform, Tm3 (Schevzov *et al.*, 2008), and in mice expressing a functional null Tm4 protein (*Tpm4*$^{Plt53/Plt53}$; Figure 2, E and F). In addition, brain and kidney masses of the Tm3 TG and *Tpm4*$^{Plt53/Plt53}$ mice were similar to those of their respective control mice (Figure 2, G and H). Collectively these data indicate an isoform-specific role for Tm5NM1 in the size of fat pads, brain, and kidney in vivo.

To assess whether the changes in TG and KO fat pad sizes were a consequence of altered proliferation of adipocytes, we measured DNA content. DNA content per whole fat pad was significantly increased in adult WAT from TG mice and decreased in the KO WAT compared with WT WAT (Figure 3, A and B, respectively). These data are consistent with changes in adipocyte cell number accounting for the changes in WAT mass in the Tm5NM1 TG and KO mice. Changes in cell proliferation in vivo were measured using the cell cycle marker Ki67 (Figure 3, C–E). The TG kidney showed a

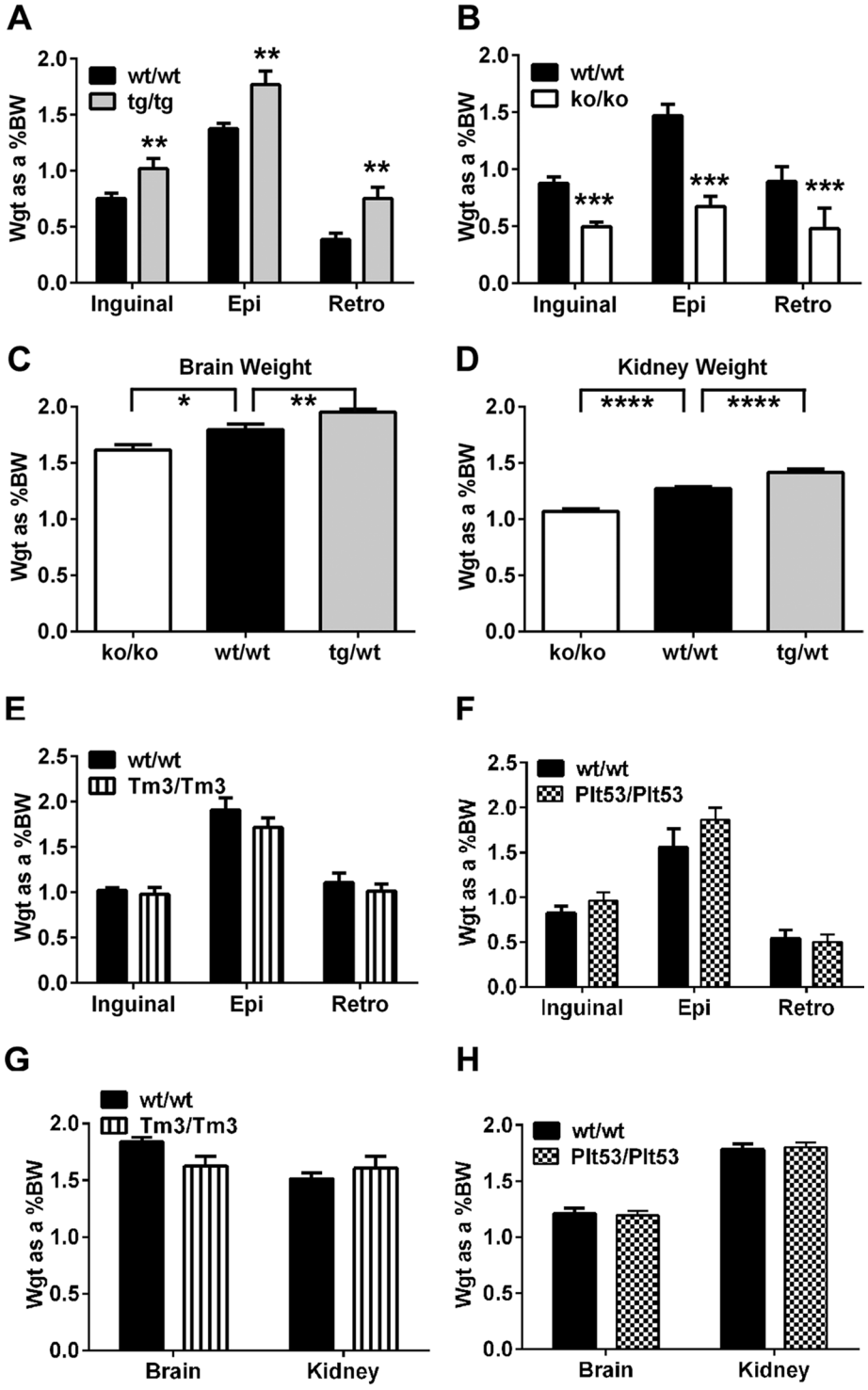

FIGURE 2: Tm5NM1 regulates organ mass. (A, B) Weight (Wgt) as a percentage of body weight (BW) of WAT depots (inguinal, epididymal [Epi], retroperitoneal [Retro] fat) from adult Tm5NM1 TG (tg/tg) and KO (ko/ko) mice compared with the corresponding strain of WT (wt/wt) controls (n = 10–15/group; 14-to 15-wk-old male mice). (C, D) Weight as a percentage of BW of brains and kidneys from adult WT (wt/wt), Tm5NM1 TG (tg/wt), and KO (ko/ko) mice (n = 9–19/group; 14-wk-old male mice). (E, F) Weight (Wgt) as a percentage of BW of WAT depots and (G, H) brains and kidneys from WT (wt/wt), Tm3 TG (Tm3/Tm3), and Tm4 functional KO (Plt53/Plt53) mice (n = 7–12/group; 15-wk-old male mice). Data are mean ± SEM. *$p < 0.05$, **$p < 0.01$, ***$p < 0.001$, ****$p < 0.0001$ (ANOVA).

significant increase in cells positive for Ki67, whereas the KO kidney trended to a reduced number of Ki67-positive cells but did not reach statistical significance (Figure 3, F and G). We conclude that the effect of Tm5NM1 on tissue and organ weight is consistent with altered cell proliferation in at least WAT and kidney and suggests that the observed effect of Tm5NM1 on MEF proliferation is of physiological significance in the mouse.

ERK regulation of cell proliferation requires Tm5NM1

Cyclin D1 expression plays a significant role in controlling cell cycle progression through the G1 phase, and its expression has been linked to signaling by the ERK subfamily of MAP kinases (Weber *et al.*, 1997). Furthermore, MAPK signaling via ERK and cyclin D1 expression is actin dependent (Bohmer *et al.*, 1996; Welsh *et al.*, 2001). Therefore to determine whether Tm5NM1 is acting through the MEK/ERK/cyclin D pathway, we examined the expression of key members of this pathway in KO and TG MEFs and adipose tissue from TG mice. Consistent with previous studies (Welsh *et al.*, 2001), we observed that addition of serum (24-h time point) to quiescent WT MEFs led to the induction of cyclin D1 expression (Figure 4). In contrast, in the KO MEFs, addition of serum (24 h) failed to increase the level of cyclin D1 expression, whereas a significant increase was observed in the TG MEFs.

The transcription factor Elk-1 is a major and direct nuclear downstream target of MAPK. Activation of the MAPK pathways and in particular ERKs results in the rapid and efficient phosphorylation and activation of Elk-1 (Yoon and Seger, 2006). Analysis of the nuclear localization of pElk-1 conducted in MEFs from both strains of mice (129/Svj and C57BL/6) showed that the KO MEFs displayed a significant reduction in the percentage of the cells with nuclear pElk-1 (Figure 4, E–H) after serum stimulation.

We conducted microarray gene expression profiling on epididymal adipose tissue of 14-wk-old TG vs. WT mice. The complete list of significantly altered genes (n = 1283) is available at the Gene Expression Omnibus (series record GSE25013). The Gene Ontology categories most significantly overrepresented (enriched) in the differentially regulated genes were Cellular Growth and Proliferation and Cell Cycle (Figure 4I). The category terms Cell Morphology and DNA Transcription were also overrepresented in the TG epididymal adipose tissue (Figure 4I). To verify the changes in cell cycle gene expression detected by the microarray, we performed quantitative real-time PCR (qRT-PCR) on cDNA synthesized from extracts of adult TG and WT control WAT (n = 10 samples/genotype). Both E2F1 and cyclin D2 (the major cyclin D isoform in fat) were significantly enhanced in the TG WAT compared with control (Figure 4J).

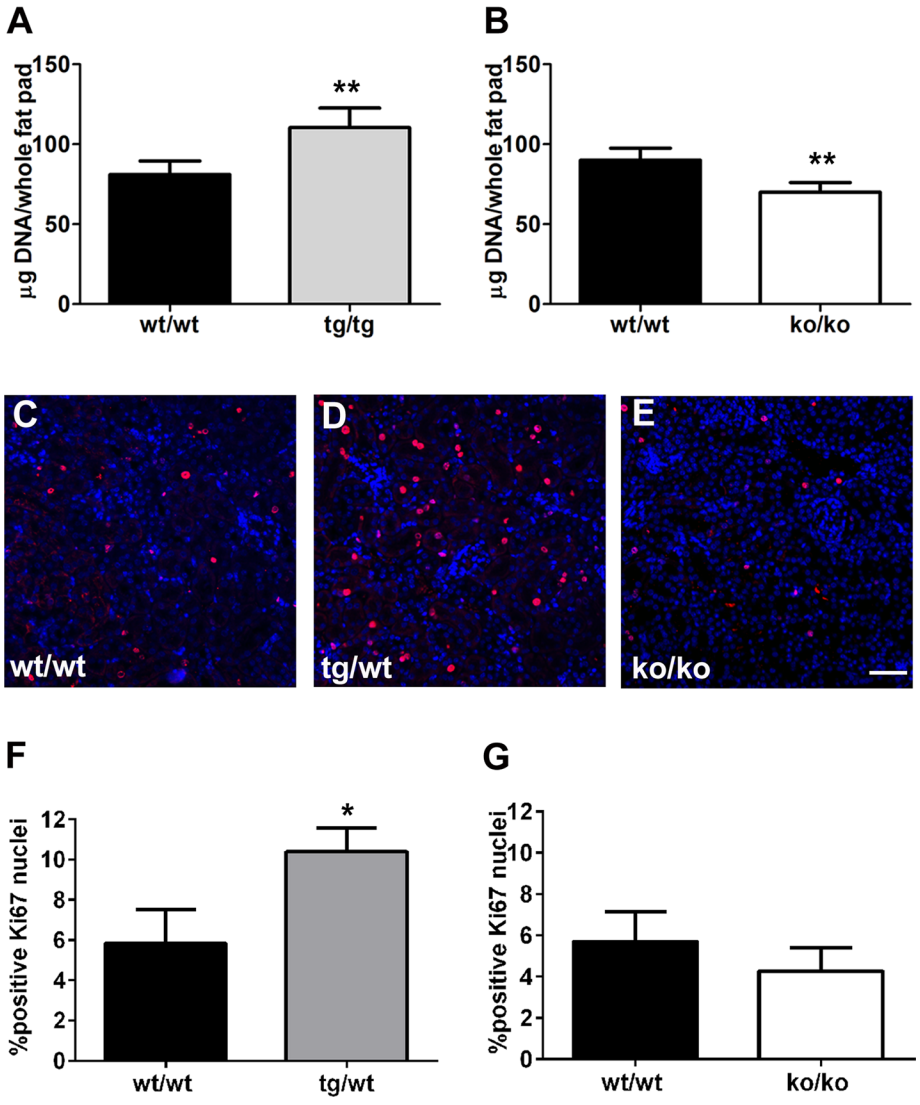

FIGURE 3: Evidence for altered cell replication in KO and TG mouse tissues. (A, B) DNA content (a measure of relative cell number) of epididymal fat pads from adult WT (wt/wt), Tm5NM1 TG (tg/tg), and KO (ko/ko) mice ($n = 6$–11/group; 14-wk-old male mice). (C–E) Representative images of kidneys isolated from the WT (wt/wt), TG (tg/wt), and KO (ko/ko) mice immunostained with the cell cycle marker Ki67 (red) and nuclear stain DAPI (blue) in 4-wk-old male mice. (F, G) Percentage of Ki67-positive nuclei determined in 4-wk-old male mice ($n = 4$ WT, $n = 5$ TG, and $n = 8$ KO). Scale bar, 50 µm. Data are mean ± SEM. *$p < 0.05$, **$p < 0.01$ (ANOVA).

proliferation rate compared with vehicle (Figure 5A). The KO MEFs were sensitive to inhibition of MEK, JNK, p38, and PI3K (Figure 5B) but completely resistant to ERK2 inhibition. We treated cells with two known ERK inhibitors, ERK inhibitor peptide 1 (Rasola *et al.*, 2010) (Figure 5B,C) and the ERK11e inhibitor (Aronov *et al.*, 2009; Figure 5, D and E), both shown to inhibit primarily ERK2. Moreover, the resistance of the KO MEFs to ERK inhibitor peptide 1 is independent of serum stimulation, as log phase (asynchronous cultures) responded in a similar manner (Figure 5F). Thus the KO MEFs have lost their ability to respond to ERK stimulation of cell proliferation.

Nuclear translocation of pERK is reduced in Tm5NM1 KO MEFs

The failure of the KO MEFs to be responsive to ERK stimulation of proliferation might be due to dysfunction at several steps in the ERK pathway. The first of these is activation of ERK by phosphorylation of its TEY motif by MEK. In agreement with previous studies (Welsh *et al.*, 2001), we observed activation of ERK after serum stimulation of synchronized MEFs (Figure 6A). The levels of pERK were unchanged in Tm5NM1 TG and KO MEFs relative to WT after serum addition (Figure 6B). No change in the expression of total ERK was detected in either the TG or KO MEFs compared with WT cells (Figure 6A).

Nuclear trafficking of pERK is essential for G1-phase cell cycle progression (Chen *et al.*, 1992; Lenormand *et al.*, 1993; Brunet *et al.*, 1999). To determine whether Tm5NM1 has a functional role in transporting pERK into the nucleus, we performed a single-cell immunofluorescence assay to visualize nuclear pERK. A gradual increase in the number of cells with nucleus-localized pERK was seen in both WT and TG, with no significant differences detected between them during the first 30 min after serum stimulation (Figure 6, C and D). In contrast, KO MEFs had a significantly reduced fraction of cells with nuclear pERK after 10 min of serum stimulation compared with WT MEFs (57 ± 1.11% vs. WT MEFs, 69 ± 0.82%; Figure 6, C and D). Although a change in nuclear pERK was detected between the WT and KO MEFs, we found that this difference was insufficient to be detected by isolation of nuclear and cytoplasmic subfractions followed by Western blotting (unpublished data). Restoration of Tm5NM1 in the KO MEFs rescued the pERK nuclear translocation defect seen in the KO MEFs (Figure 6E). This suggests a defect in the translocation of pERK to the nucleus in cells devoid of Tm5NM1.

An increase in E2F2 was also observed, although this was not statistically significant ($p = 0.07$), and there was no significant change in cyclin D1 level (Figure 4J). Taken together, these results further support the hypothesis that Tm5NM1 can influence proliferation by regulating the expression of proteins responsible for progression through the G1 phase of the cell cycle.

The importance of the MAPK family and phosphatidylinositol 3-kinase (PI3K) cascade in cell cycle progression is well documented (Chen *et al.*, 1992; Brunet *et al.*, 1999; Gera *et al.*, 2004); therefore we evaluated the potential relationship between Tm5NM1-containing filaments and these signaling cascades. Synchronized WT and Tm5NM1 TG and KO MEFs were treated with a range of MAPK and PI3K pathway inhibitors for 30 min, and cellular proliferation rates were compared. WT and TG MEFs were highly sensitive to all inhibitors, showing a significant decrease in

Tm5NM1 is required for translocation of SPS-phosphorylated pERK into the nucleus

The defect in nuclear translocation of pERK in the KO cells could be due to a lack of phosphorylation of activated pERK on the

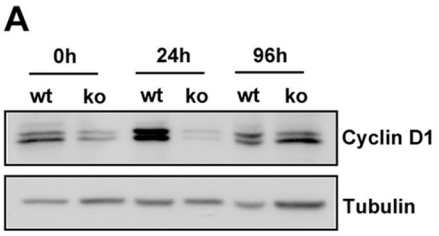

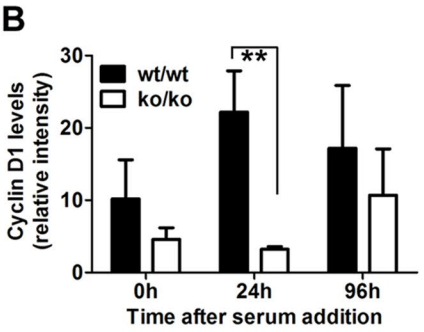

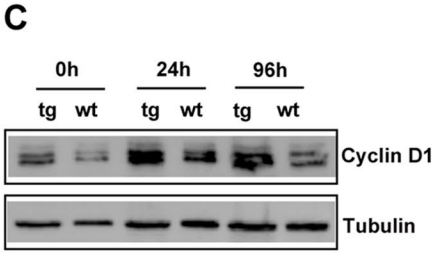

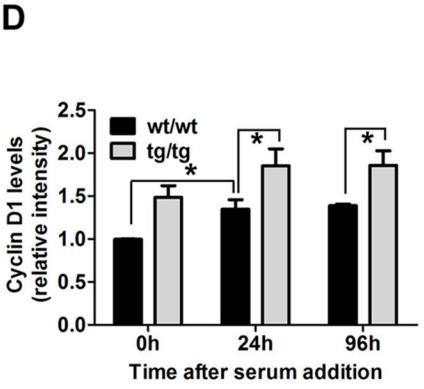

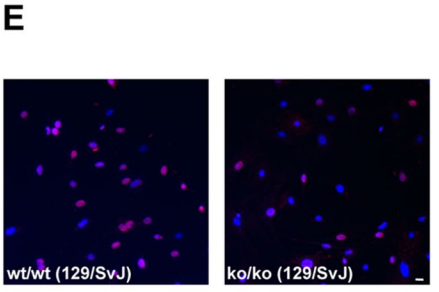

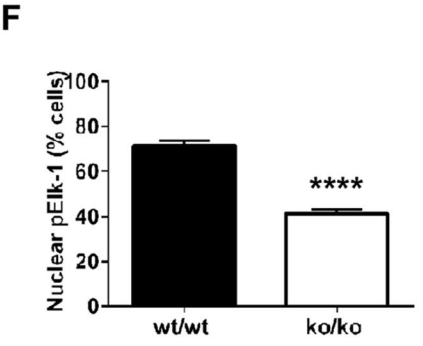

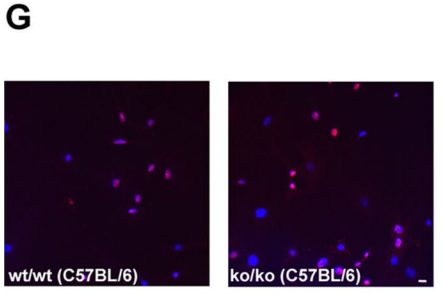

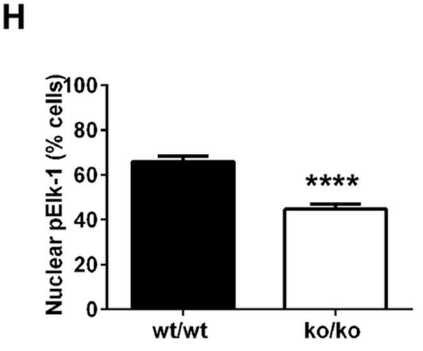

I

Functional Annotation	P value	No. transcripts
Cellular Growth and Proliferation	<0.009	283
Cell Cycle	<0.009	142
Cell Morphology	<0.009	106
Gene Expression-DNA Transcription	<0.001	109
Rho signal transduction	<0.001	10

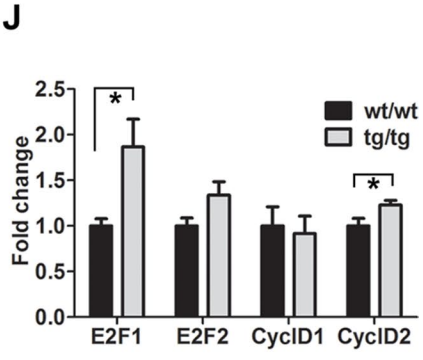

SPS site by CK2 (Plotnikov *et al.*, 2011). We observed elevated (although not statistically significant) rather than reduced levels of SPS-phosphorylated pERK in the KO cells after serum stimulation and normal levels of CK2 (Figure 7, A and B). This suggests that Tm5NM1 is acting downstream of CK2 phosphorylation of pERK and predicts that the KO cells would be insensitive to inhibition of CK2. WT and KO MEFs were treated with a CK2 inhibitor before serum stimulation. Proliferation of WT MEFs was significantly reduced by CK2 inhibition, whereas the growth of KO MEFs was unaffected compared with their respective vehicle controls (Figure 7, C and D). In addition, there was a 30% reduction in the translocation of pERK to the nucleus in serum-stimulated WT MEFs treated with the CK2 inhibitor (Figure 7E). This indicates that it is primarily the SPS-phosphorylated nuclear ERK that is responsible for ERK-stimulated cell proliferation and is significantly reduced by CK2 inhibition. The fraction of KO MEFs that were positive for nuclear pERK was similar to that of WT MEFs treated with the CK2 inhibitor, and the KO MEFs were

FIGURE 4: Evidence for changes in the expression of cyclin D, pElk-1, and E2F with altered Tm5NM1 levels. (A, C) Representative Western blots probed with cyclin D1 and α-tubulin antibodies of the 129/SvJ WT and KO MEFs and the C57BL/6 WT and TG MEFs, serum starved, and then stimulated to proliferate with the addition of serum for 24 and 96 h. (B, D) Quantification based on $n = 3$ blots using α-tubulin as loading control. *$p <$ 0.05, **$p < 0.01$. (E, G) WT (wt/wt) and KO (ko/ko) MEFs from the 129/SvJ and C57BL/6 strains of mice, were synchronized by serum starvation, followed by addition of serum for 15 min and immunofluorescence staining with pElk-1 (red). Nuclei were detected with DAPI (blue). Scale bar, 10 μm. (F, H) Percentage of cells with positive pElk-1 nuclear stain measured in the presence of 15 min of serum (>1500 cells/group). ****$p < 0.0001$. (I) Gene enrichment analysis of Illumina mRNA array data from 14-wk-old Tm5NM1 TG (tg/tg) white adipose tissue (epididymal fat) indicates that Tm5NM1 affects preferentially cell proliferation and cell cycle genes. Ingenuity Systems Analysis was performed on all transcripts shown by Illumina array analysis to be up-or down-regulated by ≥1.5 ($n = 1283$) in TG vs. WT fat. (J) Quantitative RT-PCR analysis of selected cell cycle genes of 14-wk-old TG (tg/tg) and WT (wt/wt) epididymal adipose tissue. Shown are the fold changes from WT controls. $n = 10$/group, *$p < 0.05$ (ANOVA).

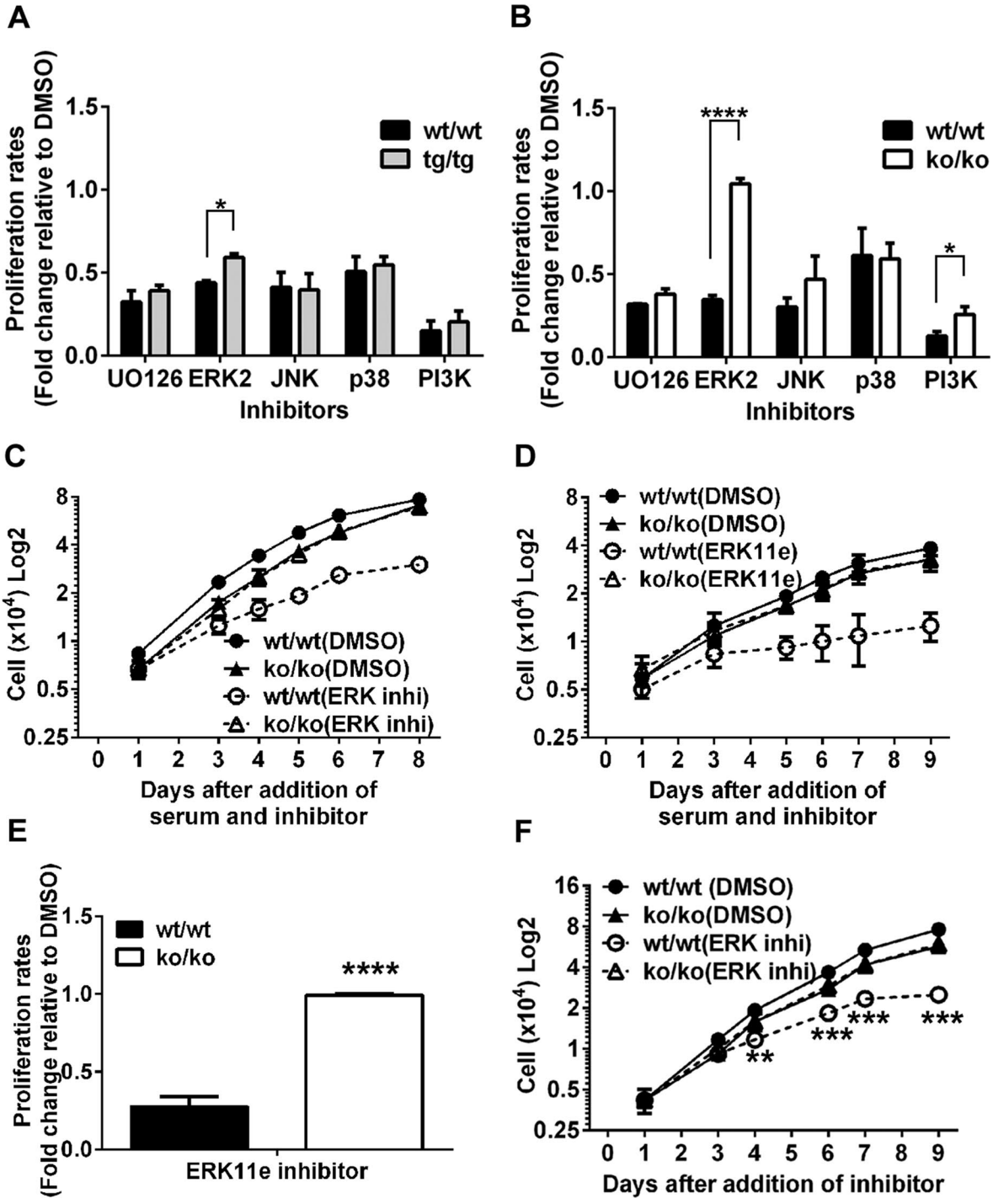

FIGURE 5: Tm5NM1 KO MEFs are refractory to ERK2 inhibition. (A, B) Serum-starved, synchronized WT (wt/wt), Tm5NM1 TG (tg/tg), and KO (ko/ko) MEFs were pretreated for 30 min with vehicle alone (DMSO) or the MEK1/2 (UO126, 2.5 μM), ERK peptide 1 (2.5 μM), JNK (JNK1/2/3, 1 μM), p38 (SB202190, 10 μM), or PI3K (LY294002, 2.5 μM) inhibitor, replated with serum, and cells counted. Proliferation rate was determined from the slope of the linear regression curves and plotted as a fold change relative to DMSO-treated MEFs. (C, D) Representative proliferation curves for serum-stimulated WT (wt/wt) and Tm5NM1 KO (ko/ko) MEFs in the presence of DMSO or ERK-specific inhibitor (peptide inhibitor 1 or ERK11e). (E) Proliferation rates of WT (wt/wt) and Tm5NM1 KO (ko/ko) MEFs in the presence of the ERK11e inhibitor determined as described in A and B. (F) Representative proliferation curves for asynchronous WT (wt/wt) and Tm5NM1 KO (ko/ko) MEFs in the presence of DMSO or the ERK-specific peptide inhibitor 1. $n = 3$, *$p < 0.05$, **$p < 0.01$, ***$p < 0.001$, ****$p < 0.0001$.

refractory to the CK2 inhibitor (Figure 7E). The data indicate that the fraction of nuclear pERK that depends on CK2 phosphorylation (pERK phosphorylated on the SPS site, referred to as pSPS-pERK) is responsible for cell proliferation and suggest that it is pSPS-pERK that is not translocated to the nucleus in the absence of Tm5NM1.

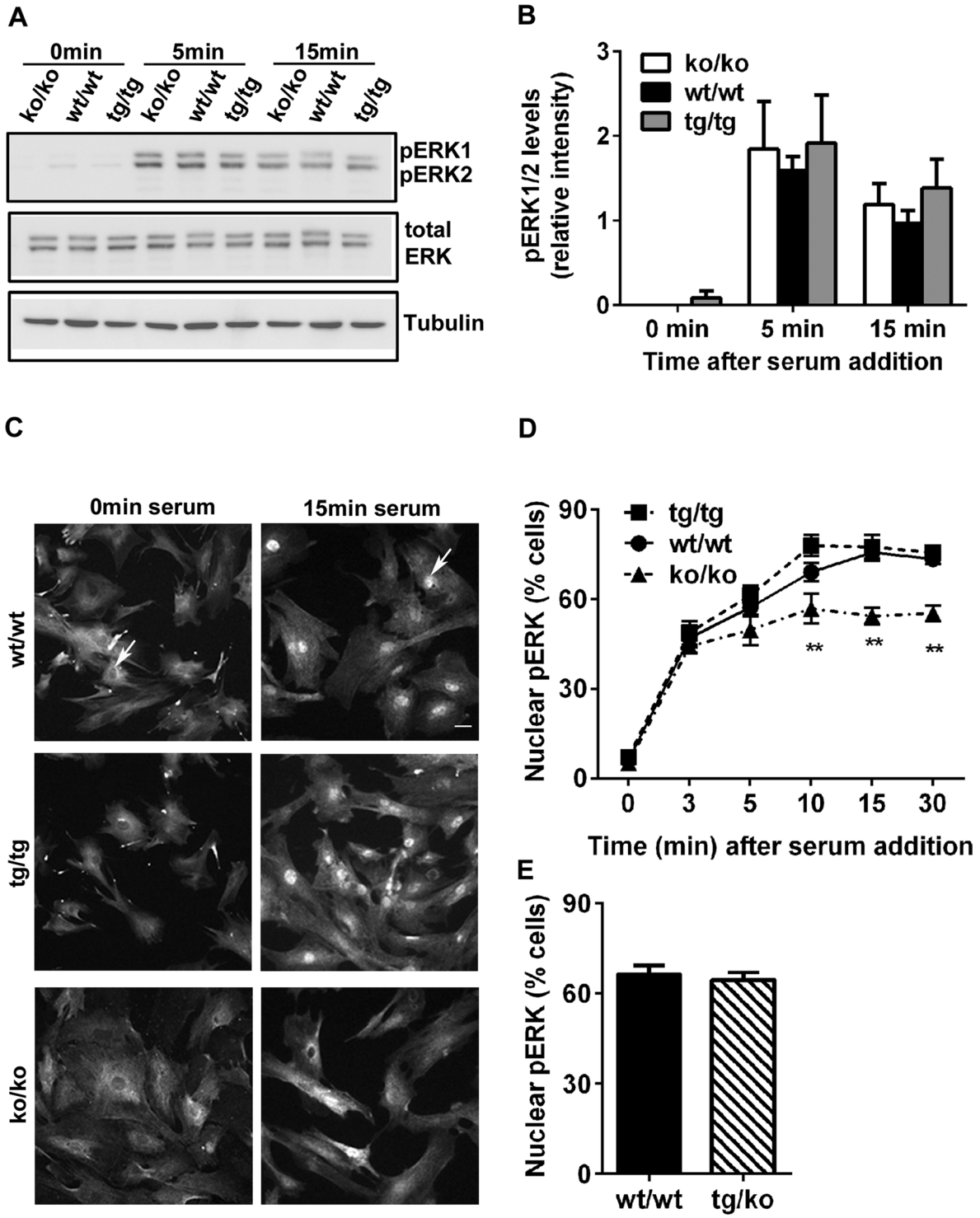

FIGURE 6: pERK nuclear translocation is impaired in Tm5NM1 KO MEFs. (A) Serum-starved WT (wt/wt), Tm5NM1 TG (tg/tg), and KO (ko/ko) MEFs were serum stimulated for 5 and 15 min and cell extracts analyzed by Western blotting using pERK, total ERK and α-tubulin (to evaluate protein loading). Representative blots are shown. (B) Quantitation of pERK. (C) WT (wt/wt), Tm5NM1 TG (tg/tg), and KO (ko/ko) MEFs were synchronized by serum starvation, followed by addition of serum for 15 min, and immunofluorescence stained with pERK. Nuclei were detected with DAPI. Arrows indicate nuclei. Scale bar, 10 μm. (D) Percentage of cells with greater nuclear pERK signal relative to cytoplasm measured in the absence, 0 min, and the presence of serum for 3, 5, 10, 15, and 30 min ($n = 3$). (E) Percentage of cells with greater nuclear pERK signal relative to cytoplasm measured in Tm5NM1 TGxKO (tg/ko) MEFs after 15 min of serum addition. $^{**}p < 0.01$.

Inhibition of WT MEFs with cytochalasin D had a similar effect on nuclear translocation of pERK to that seen in the KO MEFs (Figure 7, F and G). However, nuclear translocation of pERK in the KO MEFs was insensitive to cytochalasin D (Figure 7, F and G). This suggests that the effect of cytochalasin D on pERK nuclear translocation is dependent on Tm5NM1 and mediated by Tm5NM1-containing actin filaments.

pERK and Imp7 interactions are impaired in the absence of Tm5NM1

The simplest interpretation of these data is that Tm5NM1-containing actin filaments are required for the interaction of pERK with Imp7. To test this, we used the Duolink in situ proximity ligation assay (PLA) to evaluate the interaction of Tm5NM1 with pERK and the effect of the Tm5NM1 KO on the ability of pERK to interact with Imp7 (Soderberg *et al.*, 2006). pERK interacts with Tm5NM1 in a serum-responsive manner, with a significantly higher number of PLA signal dots in the WT MEFs after serum addition relative to serum-starved cells (Figure 8, A and C). We then examined the interaction of pERK with its nuclear shuttling protein Imp7 (Chuderland *et al.*, 2008). In WT MEFs, serum stimulation resulted in a significant increase in the number of pERK and Imp7 interactions (Figure 8, B and D). In Tm5NM1 KO MEFs, serum stimulation resulted in an increase in pERK and Imp7 interactions; however, the number of interactions was significantly lower than in the WT MEFs (Figure 8, B and D). This is not due to changes in Imp7 levels, as the WT and KO MEFs have similar levels of expression of Imp7 (Figure 8). We also confirmed that in the presence of the ERK2 inhibitor, there is a significant reduction in the number of pERK/Imp7 interactions in both the WT and KO MEFs (Figure 8G). Finally, the decrease in pERK and Imp7 interactions occurs in a Tm isoform-specific manner, as no significant change in the number of interactions between these proteins is seen in the Tm4 KO MEFs after 15-min serum stimulation (Figure 8H). This suggests that Tm5NM1-containing actin filaments are required for the association of pSPS-pERK with Imp7 and subsequent nuclear importation of pSPS-pERK to promote cell proliferation.

DISCUSSION

One of the difficulties with identifying the physiological roles of the actin cytoskeleton is that anti-actin drugs cause such widespread disruption of the cell cytoplasm that it becomes difficult to separate primary from secondary effects. In contrast, the total genetic elimination of specific tropomyosin isoforms is a potentially powerful approach to identifying the function of subsets of actin filaments containing just one or two tropomyosins in mammals (Vlahovich *et al.*, 2009; Hook *et al.*, 2011) and yeast (Drees *et al.*, 1995; Skau *et al.*, 2009; Clayton *et al.*, 2010; Coulton *et al.*, 2010). These previous studies detected the effect of tropomyosin isoforms on cell structure and myosin motor function, which is not unexpected, given the fundamental role of actin filaments in these processes. However, this report is the first to identify a role for a tropomyosin at a specific step in a signaling pathway and raises the possibility that other tropomyosin isoforms might regulate distinct steps in signaling pathways.

The MAPK signal cascade plays a vital role in cell proliferation through its ability to regulate cell cycle entry (Chen *et al.*, 1992; Lenormand *et al.*, 1993; Diehl *et al.*, 1998; Brunet *et al.*, 1999), and constitutive activation of the ERK/MAPK pathway has been identified as the driver of uncontrolled cancer cell growth (Roberts and Der, 2007). Previous studies provided evidence that actin filaments are involved in the organization of signal transduction networks, and there is increasing evidence for a direct association between actin filaments and components of the MAPK pathway (Leinweber *et al.*, 1999; Harrison *et al.*, 2004; Jongstra-Bilen and Jongstra, 2006; Ren *et al.*, 2007; White *et al.*, 2009). The specific nature of this interaction has been difficult to interpret, however, due to the use of anti-actin drugs. More recently, Dugina *et al.* (2015) showed that γ-actin, which usually contains Tpm3.1 in its filaments (Schevzov *et al.*, 1993), promotes tumorigenesis and interacts with activated ERK1/2. This aligns strongly with our results. Our identification of a specific role for Tm5NM1 in the ERK/MAPK pathway provides the opportunity to both dissect the mechanism in molecular detail and also provide an explanation for why tumors consistently retain Tm5NM1 (Stehn *et al.*, 2006, 2013)

At least two mechanisms have been identified for the nuclear translocation of ERK. Phosphorylation by CK2 on the SPS nuclear translocation sequence of pERK is vital for both passive diffusion and active transport (Chuderland *et al.*, 2008; Plotnikov *et al.*, 2011). Both passive energy-independent and active nuclear transport appear to be facilitated by the association of ERK phosphorylated on the SPS site with Imp7 (Chuderland *et al.*, 2008). In our study, WT cells were sensitive to CK2 inhibition, indicating dependence on CK2-associated phosphorylation of the SPS domain of ERK for cell proliferation. In contrast, Tm5NM1 KO MEFs were insensitive to CK2 inhibition, although phosphorylation of the SPS site of pERK is still intact. This suggests that it is the phosphorylation of the SPS nuclear translocation sequence in ERK and subsequent nuclear translocation of pSPS-pERK that is largely responsible for ERK regulation of cell proliferation in MEFs.

The results from the KO cells indicate that it is the interaction of pSPS-pERK with Imp7 that is dependent on Tm5NM1-containing actin filaments (Figure 9). There are two types of interactions that might explain this dependence on Tm5NM1. First, the interaction between pSPS-pERK and Imp7 might require Tm5NM1-containing actin filaments to facilitate their physical interaction, possibly via a scaffolding role. Second, a myosin motor might be required to physically transport pSPS-pERK to a site near the nucleus where the interaction with Imp7 can occur. We cannot discriminate between these possibilities at this time.

Knockout of Tm5NM1 was previously shown to lead to partial embryonic lethality (~50%) in two different mouse backgrounds (Hook *et al.*, 2011), and knockout of all isoforms from the gene that produces Tm5NM1 leads to complete embryonic lethality in the preimplantation embryo (Hook *et al.*, 2004). Furthermore, knockout of Tm5NM1 in mouse embryonic stem cells in cell culture results in complete lethality (Hook *et al.*, 2011). It is possible that at least some of this loss of viability might be due to the effect on ERK2 signaling. Knockout of mouse ERK2 results in complete embryonic lethality (Saba-El-Leil *et al.*, 2003; Yao *et al.*, 2003), and ERK2-knockout MEFs show reduced cell proliferation similar to that seen with the Tm5NM1 KO (Voisin *et al.*, 2010).

The finding that Tm5NM1 KO MEFs proliferate at a rate substantially greater than WT cells treated with the ERK 2 and CK2 inhibitors suggests that the KO cells shifted their reliance from pERK onto alternate signal transduction pathways to drive cell growth. There are numerous reports of cross-talk within the MAPK signaling cascades and between the MAPK and PI3K pathways in the regulation of cell survival (Mendoza *et al.*, 2011). In particular, there is strong cross-talk and compensation between the ERK/MAPK and PI3K cascades, which makes sole targeted therapy in constitutively

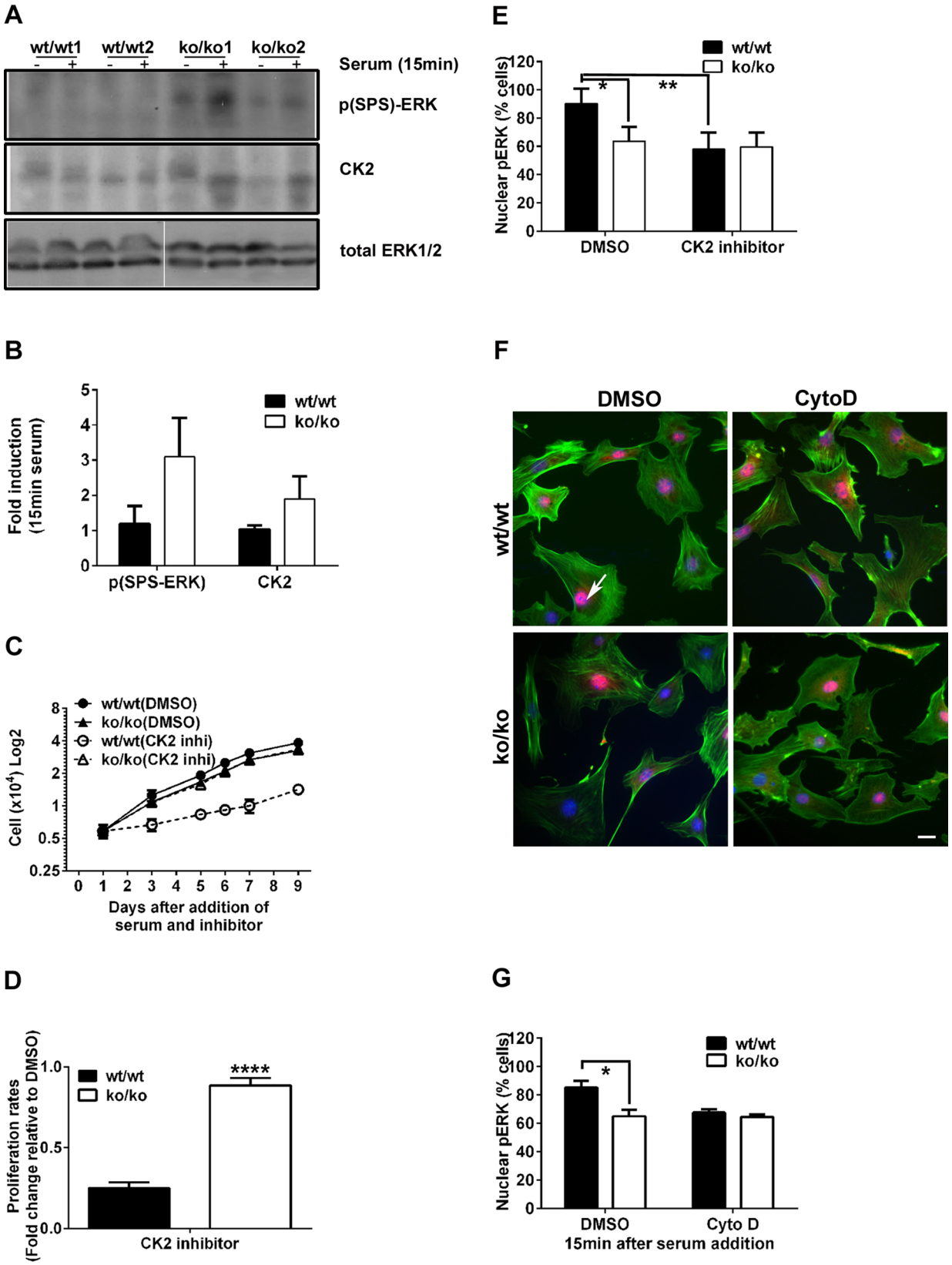

FIGURE 7: CK2 inhibition has no effect on the proliferation or nuclear translocation of pERK in the Tm5NM1 KO MEFs. (A) Serum-starved WT (wt/wt) and KO (ko/ko) MEFs, each from two separate mice, before (–) and after (+) 15 min serum stimulation were analyzed by Western blotting using p(SPS)-ERK, CK2, and total ERK (to evaluate protein loading) antibodies. (B) Fold induction in p(SPS)-EKK and CK2 determined after serum addition. *n* = 3. (C) Representative proliferation curves of serum-starved, synchronized WT (wt/wt) and Tm5NM1 KO (ko/ko) MEFs pretreated for 30 min with vehicle alone (DMSO) or CK2 inhibitor (TCMB, 0.5 μM), replated with serum, and cells counted. (D) Proliferation

activated ERK/MAPK cancers so challenging (Wee *et al.*, 2009; Villanueva *et al.*, 2010). Failure of signal transduction through one pathway leads to up-regulation of alternate pathways. To maintain proliferative capacity in the Tm5NM1 KO cells, multiple pathways within the complex network of signaling events must be providing a protective compensatory mechanism, albeit of reduced efficiency, due to the disrupted signal from ERK to the nucleus. That the KO cells have the same sensitivity to the MEK inhibitor UO126 as WT cells indicates that at least signaling downstream of MEK, but independent of ERK2, is likely to be involved. That Tm5NM1 KO MEFs are partially resistance to the PI3K inhibitor LY294002 might also reflect this reorganization of signal transduction pathway usage away from both the pERK and PI3K cascades to maximize the potential to proliferate.

We conclude that Tm5NM1 provides a nonredundant isoform-specific function essential for cell proliferation. This effect is mediated through the ERK/MAPK signaling cascade, where Tm5NM1 is essential for regulating CK2-dependent nuclear translocation of p-SPS-pERK to facilitate cell proliferation. Taking together the results presented in this study and the reported prevalence of the deregulation of the ERK pathway in numerous cancers (Roberts and Der, 2007), where Tm5NM1 is the predominant Tm isoform (Stehn *et al.*, 2006), it is possible that the antitumor effect of the recently published anti-Tm5NM1 compound might act at least in part by inhibition of the ERK/MAPK pathway in addition to its effect on the integrity of the actin cytoskeleton (Stehn *et al.*, 2013).

MATERIALS AND METHODS

Mice

Animal experiments were performed in accordance with UNSW Australia Animal Care and Ethics Committee approval and Australian National Health and Medical Research Council guidelines. The Tm5NM1 (F-Tg(*ACTB-Tpm3*.Tm5NM1)52Pgun) and Tm3 (F-Tg(*ACTB-Tpm1*.Tm3)70Pgun) TG mouse lines and Tm5NM1 (B6-*Tpm3*$^{tm2(\Delta 9d)Pgun}$) KO mouse line were reported previously (Bryce *et al.*, 2003; Kee *et al.*, 2004; Vlahovich *et al.*, 2009). The Tm5NM1 and Tm3 TG mice (FVB/N genetic background) express the human and rat forms of Tm5NM1 and Tm3, respectively, under the control of the human β-actin promoter (Schevzov *et al.*, 2008). The B6-*Tpm3*$^{tm2(\Delta 9d)Pgun}$ mouse line is a KO for both the Tm5NM1 and Tm5NM2 isoforms. However, phenotypes in this study are attributable to lack of Tm5NM1, since Tm5NM1 is the predominant or sole isoform in the cell types examined (unpublished data). Therefore, in these studies, this mouse line is termed Tm5NM1 KO. WT control mice for TG and KO mice were age-matched, of the same background strain, and bred in the same facility, and male mice were used. The Tm4 functional null mouse line (*Tpm4*$^{Plt53//Plt53}$) was identified in an *N*-ethyl-*N*-nitrosourea mutagenesis screen. This mouse line carries a single–base pair mutation that disrupts splicing, resulting in the expression of a mutant Tm4 protein that lacks the last 24 amino acids at the C-terminus and hence cannot form a polymer along the length of the actin filament (Tobacman, 2008; Martin *et al.*, 2010).

Cell culture

Primary MEFs were isolated from day 13.5 embryos and cultured as previously described (Schevzov *et al.*, 2005). WT and Tm5NM1 KO MEFs were derived from mice of two genetic backgrounds: 129/SvJ (129-*Tpm3*$^{tm1(neo;\Delta 9d)Pgun}$) and C57BL/6JArc (B6-*Tpm3*$^{tm2(\Delta 9d)Pgun}$). WT and KO MEFs from at least two embryos of each mouse strain were analyzed. Tm5NM1-overexpressing MEFs were derived from the B6.F-Tg(*ACTB-TPM3*.Tm5NM1)52Pgun line, and MEFs homozygous for the transgenic locus were used for experiments. The TG/KO MEFs were derived from a cross between the Tm5NM1 TG and the Tm5NM1 KO mice on a C57BL/6J background (B6.F-Tg(ACTB-TPM3.Tm5NM1)52Pgun × B6-Tpm3tm2(9d)Pgun). *TPM4*$^{Plt53/Plt53}$ and corresponding BALB/c WT MEFs were isolated from three littermate embryos each per genotype. Cultured cells were maintained in DMEM with 10% (vol/vol) fetal bovine serum (FBS) (Invitrogen, Life Technologies, Melbourne, Australia) at 37°C and 5% CO_2. DNA content was analyzed by flow cytometry after propidium iodide staining (FACs Canto II flow cytometer; BD). G0/G1, S, and G2/M cell cycle phases were quantified with FACs Diva software.

Proliferation assays

MEFs were initially arrested in the G1/S phase of the cell cycle by culturing cells in DMEM containing 0.1% (vol/vol) FBS for 72 h. Cells (1×10^4/well) were seeded onto a 24-well plate in the presence of DMEM supplemented with 10% (vol/vol) FBS to allow reentry into the cell cycle. Cells were counted using a hemocytometer. For inhibitor studies, synchronized cells were treated with inhibitors for 30 min while suspended in trypsinization medium before plating in the presence of DMEM containing 10% (vol/vol) FBS. LY294002 (2.5 μM), U0126 (2.5 μM), ERK Activation Inhibitor Peptide 1 (2.5 μM), JNK Inhibitor I (L)-Form (1 μM), and SB202190 (10 μM) were purchased from Calbiochem, Merck Millipore, Melbourne, Australia. ERK11e (50 nM) and 2-(4,5,6,7-tetrabromo-2-(dimethylamino)-1*H*-benzo[*d*]imidazol-1-yl)acetic acid (TMCB) CK2 (0.5 μM) inhibitors were from Tocris Biosciences (Bristol, UK).

5-Ethynyl-2′-deoxyuridine incorporation

WT and KO MEFs were serum starved as described and seeded onto matrix-coated acrylamide hydrogels (0.03–0.3% acrylamide; Klein *et al.*, 2007, 2009). S-phase entry was determined by measuring 5-ethynyl-2′-deoxyuridine incorporation (Klein *et al.*, 2007).

rate of WT (wt/wt) and Tm5NM1 KO (ko/ko) MEFs exposed to the CK2 inhibitor determined from the slope of the linear regression curves and plotted as fold change relative to DMSO vehicle control. $n = 3$, ****$p < 0.0001$. (E) Nuclear translocation of pERK determined in serum-starved WT (wt/wt) and Tm5NM1 KO (ko/ko) MEFs pretreated with vehicle alone (DMSO) or TMCB (CK2 inhibitor; 0.5 μM, 2 h), followed by 15 min of serum stimulation before fixing and treatment with the pERK antibody. (F) WT (wt/wt) and Tm5NM1 KO (ko/ko) MEFs were serum starved for 24 h and exposed for 90 min to DMSO or 500 nM cytochalasin D, followed by serum addition for 15 min. Cells were fixed and immunostained with pERK1/2 (red) and phalloidin (green) to confirm the effect of cytochalasin D. Nuclei were detected with DAPI. Arrow indicates pERK-positive nucleus. Scale bar, 10 μm. (G) Nuclear translocation of pERK quantitated as in E. $n = 3$; *$p < 0.05$, **$p < 0.01$, ****$p < 0.0001$.

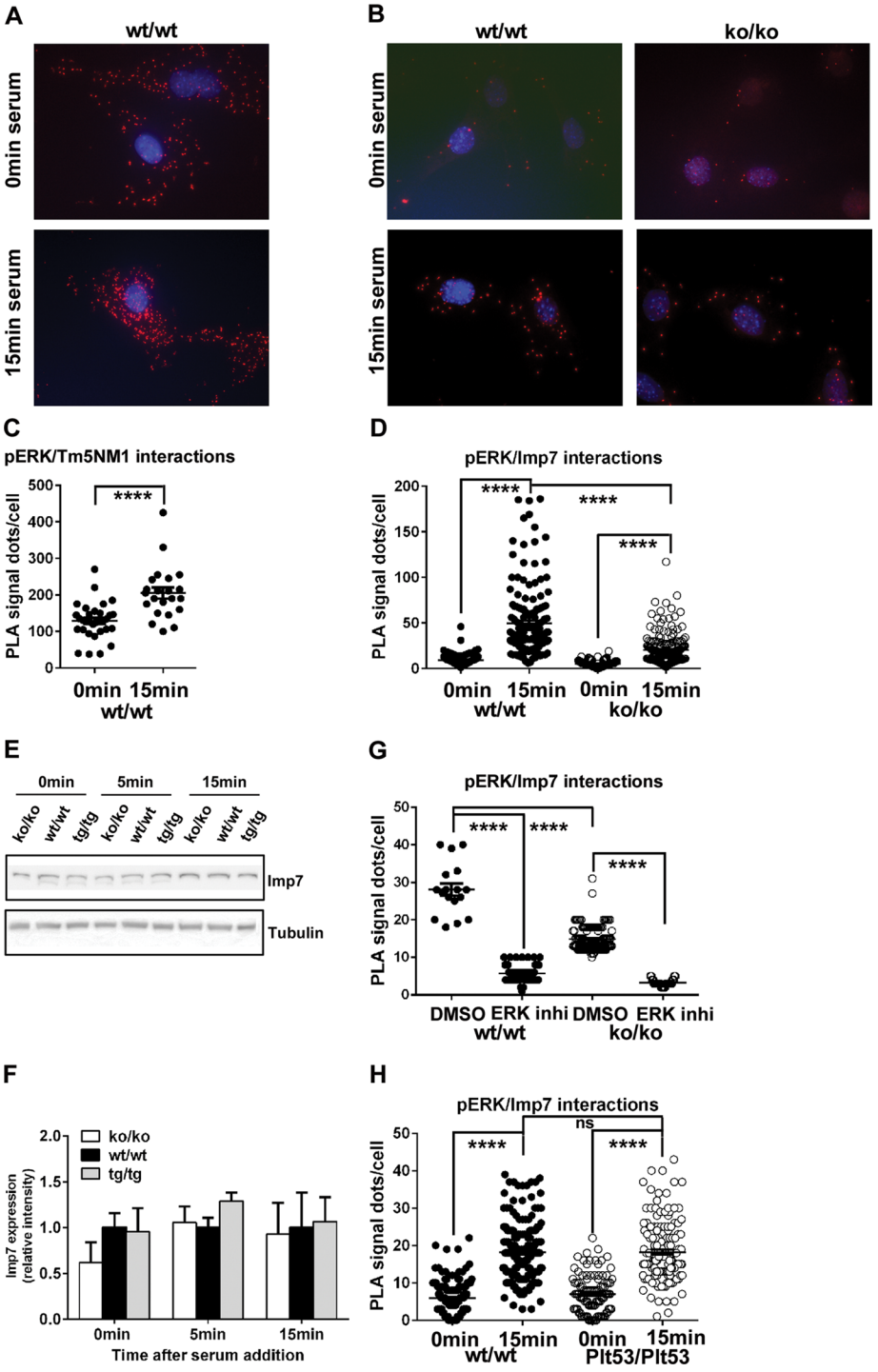

FIGURE 8: Tm5NM1 is required for efficient interaction of pERK with Imp7. (A) WT (wt/wt) MEFs were synchronized by serum starvation, followed by addition of serum for 15 min, and the Duolink PLA was performed to detect pERK and Tm5NM1 interactions. Nuclei are detected with DAPI. (B) WT (wt/wt) and Tm5NM1 KO (ko/ko) MEFs were synchronized by serum starvation, followed by addition of serum for 15 min, and the Duolink PLA was performed to detect pERK1/2 and Imp7 interactions. Nuclei were detected with DAPI. Scale bar, 10 μm. (C, D) Number of pERK/Tm5NM1 or pERK/Imp7 interactions quantitated using Image J. $n = 3$; ****$p < 0.0001$. (E) Serum-starved WT (wt/wt), Tm5NM1 TG (tg/tg), and KO (ko/ko) MEFs were stimulated to proliferate with the addition of serum for 0, 5, and 15 min. Cell extracts were analyzed by Western blotting using antibodies to Imp7 and α-tubulin (to evaluate protein loading). Representative blots. (F) Quantification of Imp7 levels using α-tubulin as loading control ($n = 3$). WT was set at 1. (G) Serum-starved, synchronized WT (wt/wt) and Tm5NM1 KO (ko/ko) MEFs were pretreated for 30 min with vehicle alone (DMSO) or the ERK11e inhibitor (50 nM), followed by addition of serum for 15 min, and the Duolink PLA performed to examine pERK1/2 and Imp7 interactions. (H) WT (wt/wt) and Tm4 functional KO (Plt53/Plt53) MEFs were treated as described in B, and the Duolink PLA was performed to examine pERK1/2 and Imp7 interactions. The number of interactions was quantitated using ImageJ ($n = 3$). Nuclei were detected with DAPI. ****$p < 0.0001$.

Western blotting

Mouse adipose tissue was prepared as previously described (Schevzov *et al.*, 2008). Cell lysates were harvested in radioimmunoprecipitation assay (RIPA) buffer (20 mM Tris, pH 7.4, 150 mM sodium chloride, 1% [vol/vol] Nonidet P-40, 0.5% [vol/vol] sodium deoxycholate, 1 mM EDTA, 0.1% [vol/vol] SDS, Complete Mini Protease Inhibitor EDTA free tablet [Roche Diagnostics], and PhosSTOP phosphatase inhibitor cocktail tablet [Roche Diagnostics]). Antibodies used included α/9d (mouse monoclonal; Tm1, 2, 3, 5a, 5b, 6), γ/9d (sheep polyclonal; Tm5NM1; Schevzov *et al.*, 2005), LC1 (mouse and human Tm5NM1; Sung *et al.*, 2000), CG3 (Novy *et al.*, 1993), δ/9d (rabbit polyclonal; Tm4; Hannan *et al.*, 1998), and δ/1b (mouse monoclonal; Tm4; Schevzov *et al.*, 2011). Also used were phospho–p44/p42 MAPK (ERK1/2; Thr-202/Tyr-204), total p44/p42 MAPK (ERK1/2) and cyclin D1 (A-12) antibodies (Cell Signaling Technology, via Genesearch, Brisbane, Australia), anti–phospho-SPS-ERK (obtained from Rony Seger, Weizmann Institute of Science, Rehovot, Israel), α-tubulin (clone DM 1A) antibody (Sigma-Aldrich, Sydney, Australia) and Imp7 IPO7 monoclonal antibody (M07), clone 4G6 (Sapphire Biosciences, Sydney, Australia). Anti-rabbit, anti-sheep, and anti-mouse immunoglobulin G–conjugated horseradish peroxidase secondary antibodies were from GE Healthcare, Sydney, Australia. Western blots were quantified using ImageJ software (National Institutes of Health, Bethesda, MD).

Body fat and adipose tissue analysis

After starvation for 14-16 h, total body fat and lean tissue composition of male mice (14–15 wk old) was assessed using a Mouse GE Lunar PIXImus densitometer (GE Healthcare; MacArthur *et al.*, 2008). DNA content of epididymal adipose tissue of 14- to 15-wk-old mice after 14–16 h of starvation (n = 8/group) was determined as previously reported (Labarca and Paigen, 1980).

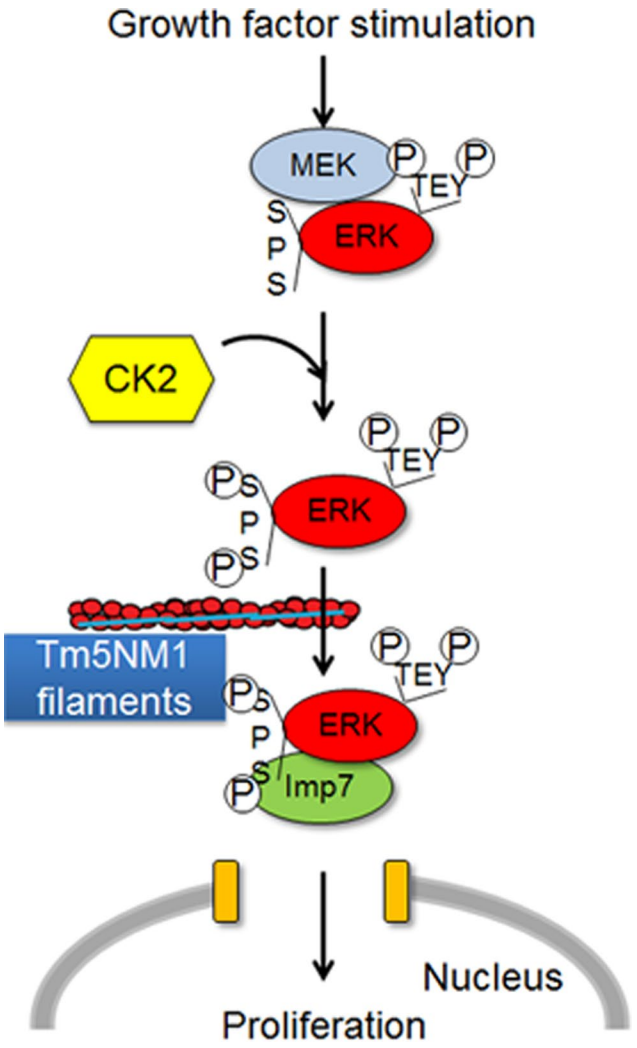

FIGURE 9: Model proposing a potential role for Tm5NM1-containing actin filaments in ERK nuclear translocation. On growth factor stimulation, ERK is phosphorylated on the TEY site by MEK, followed by further phosphorylation on the nuclear translocation signal (SPS) primarily by CK2. We postulate that Tm5NM1-containing actin filaments are required to coordinate interaction between pSPS-pERK and Imp7, possibly via function as a scaffold and/or recruitment of a myosin motor to assist in the physical transportation of pSPS-pERK through the cytoplasm to interact with Imp7.

Illumina BeadArray analysis

Gene expression profiling was performed on epididymal adipose tissue from Tm5NM1 TG and WT control mice (14- to 16-h–fasted, 4-mo-old male mice; n = 5 and 4/group, respectively) using Illumina (Scoresby) 46K mouse BeadArrays as previously outlined (Pearen *et al.*, 2009). RNA was purified using a mini-RNeasy kit (Qiagen, Sydney, Australia) according to the manufacturer's instructions. Integrity of the total RNA samples was assessed using the Agilent Bioanalyzer 2100, and RNA integrity scores >7.8 were present in all samples. Amplified cRNA (1.5 µg) was hybridized to Sentrix Mouse-6.v1 BeadChip arrays (Illumina, San Diego, CA). BeadChip arrays (Accession GPL6283) were scanned with an Illumina BeadStation Scanner and the data imported into Gene-Spring GX v7.3.1 software (Agilent, Santa Clara, CA) for data analysis. Data were normalized to control genes, genes with an Illumina detection score equal to 1, and all probes except the genes with an Illumina detection score equal to 1 were filtered out to remove probes without adequate expression levels. A parametric Welsh test (unequal variance) was performed (p cut-off of 0.05), and multiple testing correction (Benjamini and Hochberg false discovery rate) was then applied to genes that passed the Welch test (PASW Statistics 18 software; SPSS). After the statistical filtering, 70 genes were found to be changed by ≥2.0-fold and 483 by ≥1.75-fold. Ingenuity Pathway Analysis (www.ingenuity.com) was performed on genes with positive or negative fold changes between TG and WT tissue of >1.5 (1283 transcripts).

qRT-PCR analysis

RNA was extracted from epididymal adipose tissue using TRI-Reagent (Sigma-Aldrich) and further purified using a mini-RNeasy kit (Qiagen). cDNA was synthesized from 1 µg of total RNA using M-MLV Reverse Transcriptase (Promega, Sydney, Australia) primed by random hexamers, according to the manufacturer's instructions. qRT-PCR was performed on epididymal adipose tissue (n = 10/group). The primers were either purchased from Qiagen or designed using the Primer 3 Input (version 4.0) or Primer-Blast (National Center for Biotechnology Information); see Supplemental Table S1 for primer sequences). PCR was performed in a final volume of 20 µl, consisting of diluted cDNA sample, 1× Brilliant II SYBR Green QPCR Master Mix (Stratagene, via Integrated Sciences, Sydney, Australia), primers optimized for each target gene, and nuclease-free water. qRT-PCR was performed using a Mx300P machine (Stratagene) and was conducted over 40 cycles of 95°C for 30 s, 60°C for 1 min, and 72°C for 1 min preceded by an initial 95°C for 10 min. Relative quantities of target transcripts were calculated from triplicate samples after normalization of the data against *HPRT* using the standard curve method. For each target gene, qRT-PCR was performed at least twice. TG versus WT mice were compared using two-tailed Student's t test assuming unequal variances.

Immunofluorescence

MEFs were plated onto glass chamber slides and immunostained with pERK1/2 (Aplin *et al.*, 2001), followed by donkey/anti-rabbit/555 antibody (Jackson ImmunoResearch Laboratories, West Grove, PA). Phospho–Elk-1 (Ser-383) (Cell Signaling Technology) immunostaining was conducted after fixation of the cells in 4% (vol/vol) paraformaldehyde and blocking of nonspecific binding; dilution of the antibody (1/500) was in 1% (vol/vol) bovine serum albumin (BSA), 10% (vol/vol) normal goat serum, and 0.1% (vol/vol) Triton X-100. The cytochalasin D (Sigma-Aldrich) experiment was conducted by first seeding and culturing cells for 24 h, serum starving them for 24 h, and treating them for 90 min with cytochalasin D (500 nM) or dimethyl sulfoxide (DMSO). MEFs were fixed and stained with phalloidin ATTO 488 (ATTO-TEC, Siegen, Germany) as previously described (Schevzov *et al.*, 2008). Coverslips were mounted using FluorSave Reagent (Calbiochem). Images were captured with a Zeiss Axioskop 40 FL (Carl Zeiss, Oberkochen, Germany) using the 40×/0.65 numerical aperture (NA) or 10×/0.25NA objectives and photographed using a Zeiss AxioCam MRc charge-coupled device (CCD) camera.

Kidneys were dissected from 4-wk-old Tm5NM1 TG (n = 5), WT (n = 4), and KO (n = 8) mice, all on a C57BL6 background. Kidneys were fixed in 10% neutral buffered Formalin and embedded in paraffin using an Excelsior tissue processor (Thermo Scientific, Melbourne, Australia) and sectioned at 4 µm. Antigen retrieval was performed in 10 mM citrate buffer, pH 5.8, in an RHS-1 microwave

vacuum histoprocessor (Milestone, Kalamazzo, MI) at 120°C. Sections were blocked in 5% goat serum, 5% FBS, and 1% BSA for 2 h at room temperature and incubated overnight at room temperature with a Ki67 rabbit polyclonal antibody (SP6, 1:200; Novus Biologicals). Secondary antibody (1:750; ImmunoResearch Laboratories) coupled with the fluorochrome Alexa Fluor 555 was diluted in blocking buffer. Nuclei were visualized with 4′,6-diamidino-2-phenylindole (DAPI; 1:10,000, Molecular Probes, Life Technologies, Melbourne, Australia). Images were captured with a BX51 fluorescence microscope equipped with a DP73 CCD color camera (Olympus). Ki67-positive nuclei in kidney cortical tubules were counted and normalized to total nuclei (DAPI stained). Nuclei were counted in three random fields (2000 nuclei/field) per kidney where proliferation was evident using ImageJ software.

Proximity ligation assay

Intracellular protein–protein interactions were examined using the Duolink PLA kit (Olink Biosciences, Sigma-Aldrich). In brief, cells were cultured and serum starved as described, fixed with 4% paraformaldehyde, and permeabilized with 0.1% (vol/vol) Triton X-100 in phosphate-buffered saline. Primary antibodies were incubated overnight at 4°C and samples processed according to the instructions provided. The red PLA signal dots were visualized using a Zeiss Axioskop 40 FL (Carl Zeiss), photographed using a Zeiss AxioCam MRc CCD camera, and quantitated using ImageJ.

Statistical analysis

Statistical analysis of the BeadArray data was as described. All other experimental data are expressed as mean ± SEM for $n \geq 3$ experiments. Provided the data passed the D'Agnostino and Perron test for Gaussian distribution (PASW Statistics 18), significant difference between groups was determined by a two-tailed Student's *t* test assuming unequal variances for comparisons between two groups or by a one-way analysis of variance (ANOVA) followed by Tukey's posthoc for more than two groups. If data did not fit a Gaussian distribution or group sizes were small ($n < 5$), the nonparametric Kruskal–Wallis test was performed to determine significance between groups. For intergroup comparisons of greater than two, a Dunn multiple comparison test was performed (PASW Statistics). $p < 0.05$ was considered statistically significant. *$p < 0.05$, **$p < 0.01$, ***$p < 0.001$, and ****$p < 0.0001$.

ACKNOWLEDGMENTS

We thank Renee Szokolai, Melissa Desouza, and Shane Whittaker for technical assistance and Nicole Bryce for critical reading of the manuscript. This work was supported by Project Grants APP1004175 and APP570762 from the Australian National and Medical Research Council (P.W.G., G.S., and E.C.H. and P.W.G., E.C.H., and A.J.K., respectively) and funding from the Kids Cancer Project. A.J.K. and J.R.S. are Kids Cancer Project, Childhood Cancer Cytoskeletal Consortium (C4) Research Fellows. J.D.C. was supported by the Medical Foundation of the University of Sydney. E.A.M. was a Cancer Institute NSW Fellow. P.W.G. was a Principal Research Fellow of the Australian National and Medical Research Council (163626). B.T.K. was supported by a Program Grant (1016647), an Independent Research Institutes Infrastructure Support Scheme Grant (361646) from the National and Medical Research Council, and a fellowship from the Sylvia and Charles Viertel Foundation. I.P. was supported by a fellowship from the Deutsche Forschungsgemeinschaft. This work was also supported by the Australian Cancer Research Fund and a Victorian State Government Operational Infrastructure Support Grant.

REFERENCES

Aplin AE, Stewart SA, Assoian RK, Juliano RL (2001). Integrin-mediated adhesion regulates ERK nuclear translocation and phosphorylation of Elk-1. J Cell Biol 153, 273–282.

Aronov AM, Tang Q, Martinez-Botella G, Bemis GW, Cao J, Chen G, Ewing NP, Ford PJ, Germann UA, Green J, *et al.* (2009). Structure-guided design of potent and selective pyrimidylpyrrole inhibitors of extracellular signal-regulated kinase (ERK) using conformational control. J Med Chem 52, 6362–6368.

Assoian RK, Klein EA (2008). Growth control by intracellular tension and extracellular stiffness. Trends Cell Biol 18, 347–352.

Atten MJ, Attar BM, Holian O (1998). Cytoskeletal PKC and ERK/MAPK activation in response to N-nitrosamines and phorbol 12-myristate 13-acetate in gastric adenocarcinoma cells. Anticancer Res 18, 4377–4382.

Bohmer RM, Scharf E, Assoian RK (1996). Cytoskeletal integrity is required throughout the mitogen stimulation phase of the cell cycle and mediates the anchorage-dependent expression of cyclin D1. Mol Biol Cell 7, 101–111.

Brunet A, Roux D, Lenormand P, Dowd S, Keyse S, Pouyssegur J (1999). Nuclear translocation of p42/p44 mitogen-activated protein kinase is required for growth factor-induced gene expression and cell cycle entry. EMBO J 18, 664–674.

Bryce NS, Schevzov G, Ferguson V, Percival JM, Lin JJ, Matsumura F, Bamburg JR, Jeffrey PL, Hardeman EC, Gunning P, *et al.* (2003). Specification of actin filament function and molecular composition by tropomyosin isoforms. Mol Biol Cell 14, 1002–1016.

Bunnell TM, Ervasti JM (2011). Structural and functional properties of the actin gene family. Crit Rev Eukaryot Gene Expr 21, 255–266.

Chen RH, Sarnecki C, Blenis J (1992). Nuclear localization and regulation of erk-and rsk-encoded protein kinases. Mol Cell Biol 12, 915–927.

Chuderland D, Konson A, Seger R (2008). Identification and characterization of a general nuclear translocation signal in signaling proteins. Mol Cell 31, 850–861.

Clayton JE, Sammons MR, Stark BC, Hodges AR, Lord M (2010). Differential regulation of unconventional fission yeast myosins via the actin track. Curr Biol 20, 1423–1431.

Coulton AT, East DA, Galinska-Rakoczy A, Lehman W, Mulvihill DP (2010). The recruitment of acetylated and unacetylated tropomyosin to distinct actin polymers permits the discrete regulation of specific myosins in fission yeast. J Cell Sci 123, 3235–3243.

Diehl JA, Cheng M, Roussel MF, Sherr CJ (1998). Glycogen synthase kinase-3beta regulates cyclin D1 proteolysis and subcellular localization. Genes Dev 12, 3499–3511.

Drees B, Brown C, Barrell BG, Bretscher A (1995). Tropomyosin is essential in yeast, yet the TPM1 and TPM2 products perform distinct functions. J Cell Biol 128, 383–392.

Dugina V, Khromova N, Rybko V, Blizniukov O, Shagieva G, Chaponnier C, Kopnin B, Kopnin P (2015). Tumor promotion by γ and suppression by β non-muscle actin isoforms. Oncotarget. PMID: 26008973.

Dugina V, Zwaenepoel I, Gabbiani G, Clement S, Chaponnier C (2009). Beta and gamma-cytoplasmic actins display distinct distribution and functional diversity. J Cell Sci 122, 2980–2988.

Gera JF, Mellinghoff IK, Shi Y, Rettig MB, Tran C, Hsu JH, Sawyers CL, Lichtenstein AK (2004). AKT activity determines sensitivity to mammalian target of rapamycin (mTOR) inhibitors by regulating cyclin D1 and c-myc expression. J Biol Chem 279, 2737–2746.

Gunning P, O'Neill G, Hardeman E (2008). Tropomyosin-based regulation of the actin cytoskeleton in time and space. Physiol Rev 88, 1–35.

Hannan AJ, Gunning P, Jeffrey PL, Weinberger RP (1998). Structural compartments within neurons: developmentally regulated organization of microfilament isoform mRNA and protein. Mol Cell Neurosci 11, 289–304.

Harrison RE, Sikorski BA, Jongstra J (2004). Leukocyte-specific protein 1 targets the ERK/MAP kinase scaffold protein KSR and MEK1 and ERK2 to the actin cytoskeleton. J Cell Sci 117, 2151–2157.

Hendricks M, Weintraub H (1984). Multiple tropomyosin polypeptides in chicken embryo fibroblasts: differential repression of transcription by Rous sarcoma virus transformation. Mol Cell Biol 4, 1823–1833.

Hook J, Lemckert F, Qin H, Schevzov G, Gunning P (2004). Gamma tropomyosin gene products are required for embryonic development. Mol Cell Biol 24, 2318–2323.

Hook J, Lemckert F, Schevzov G, Fath T, Gunning P (2011). Functional identity of the gamma tropomyosin gene: Implications for embryonic development, reproduction and cell viability. Bioarchitecture 1, 49–59.

Huang S, Chen CS, Ingber DE (1998). Control of cyclin D1, p27(Kip1), and cell cycle progression in human capillary endothelial cells by cell shape and cytoskeletal tension. Mol Biol Cell 9, 3179–3193.

Huang S, Ingber DE (2002). A discrete cell cycle checkpoint in late G(1) that is cytoskeleton-dependent and MAP kinase (Erk)-independent. Exp Cell Res 275, 255–264.
Johnson M, East DA, Mulvihill DP (2014). Formins determine the functional properties of actin filaments in yeast. Curr Biol 24, 1525–1530.
Jongstra-Bilen J, Jongstra J (2006). Leukocyte-specific protein 1 (LSP1): a regulator of leukocyte emigration in inflammation. Immunol Res 35, 65–74.
Kee AJ, Schevzov G, Nair-Shalliker V, Robinson CS, Vrhovski B, Ghoddusi M, Qiu MR, Lin JJ, Weinberger R, Gunning PW, *et al.* (2004). Sorting of a nonmuscle tropomyosin to a novel cytoskeletal compartment in skeletal muscle results in muscular dystrophy. J Cell Biol 166, 685–696.
Klein EA, Yin L, Kothapalli D, Castagnino P, Byfield FJ, Xu T, Levental I, Hawthrone E, Janmey PA, Assoian RK (2009). Cell-cycle control by physiological matrix elasticity and in vivo tissue stiffening. Curr Biol 19, 1511–1518.
Klein EA, Yung Y, Castagnino P, Kothapalli D, Assoian RK, David AC (2007). Cell adhesion, cellular tension, and cell cycle control. Methods Enzymol 426, 155–175.
Labarca C, Paigen K (1980). A simple, rapid, and sensitive DNA assay procedure. Anal Biochem 102, 344–352.
Leinweber BD, Leavis PC, Grabarek Z, Wang CL, Morgan KG (1999). Extracellular regulated kinase (ERK) interaction with actin and the calponin homology (CH) domain of actin-binding proteins. Biochem J 344, 117–123.
Lenormand P, Sardet C, Pages G, L'Allemain G, Brunet A, Pouyssegur J (1993). Growth factors induce nuclear translocation of MAP kinases (p42mapk and p44mapk) but not of their activator MAP kinase kinase (p45mapkk) in fibroblasts. J Cell Biol 122, 1079–1088.
Lin JJ, Helfman DM, Hughes SH, Chou CS (1985). Tropomyosin isoforms in chicken embryo fibroblasts: purification, characterization, and changes in Rous sarcoma virus-transformed cells. J Cell Biol 100, 692–703.
MacArthur DG, Seto JT, Chan S, Quinlan KG, Raftery JM, Turner N, Nicholson MD, Kee AJ, Hardeman EC, Gunning PW, *et al.* (2008). An Actn3 knockout mouse provides mechanistic insights into the association between alpha-actinin-3 deficiency and human athletic performance. Hum Mol Genet 17, 1076–1086.
Martin C, Schevzov G, Gunning P (2010). Alternatively spliced N-terminal exons in tropomyosin isoforms do not act as autonomous targeting signals. J Struct Biol 170, 286–293.
McNicol A, Shibou TS, Pampolina C, Israels SJ (2001). Incorporation of map kinases into the platelet cytoskeleton. Thromb Res 103, 25–34.
Mendoza MC, Er EE, Blenis J (2011). The Ras-ERK and PI3K-mTOR pathways: cross-talk and compensation. Trends Biochem Sci 36, 320–328.
Michelot A, Drubin DG (2011). Building distinct actin filament networks in a common cytoplasm. Curr Biol 21, R560–R569.
Nithianandarajah-Jones GN, Wilm B, Goldring CE, Muller J, Cross MJ (2012). ERK5: structure, regulation and function. Cell Signal 24, 2187–2196.
Novy RE, Sellers JR, Liu LF, Lin JJ (1993). In vitro functional characterization of bacterially expressed human fibroblast tropomyosin isoforms and their chimeric mutants. Cell Motil Cytoskel 26, 248–261.
O'Neill GM, Stehn J, Gunning PW (2008). Tropomyosins as interpreters of the signalling environment to regulate the local cytoskeleton. Semin Cancer Biol 18, 35–44.
Pearen MA, Ryall JG, Lynch GS, Muscat GE (2009). Expression profiling of skeletal muscle following acute and chronic beta2-adrenergic stimulation: implications for hypertrophy, metabolism and circadian rhythm. BMC Genomics 10, 448.
Percival JM, Thomas G, Cock TA, Gardiner EM, Jeffrey PL, Lin JJ, Weinberger RP, Gunning P (2000). Sorting of tropomyosin isoforms in synchronised NIH 3T3 fibroblasts: evidence for distinct microfilament populations. Cell Motil Cytoskel 47, 189–208.
Plotnikov A, Chuderland D, Karamansha Y, Livnah O, Seger R (2011). Nuclear extracellular signal-regulated kinase 1 and 2 translocation is mediated by casein kinase 2 and accelerated by autophosphorylation. Mol Cell Biol 31, 3515–3530.
Rasola A, Sciacovelli M, Chiara F, Pantic B, Brusilow WS, Bernardi P (2010). Activation of mitochondrial ERK protects cancer cells from death through inhibition of the permeability transition. Proc Natl Acad Sci USA 107, 726–731.
Ren JG, Li Z, Sacks DB (2007). IQGAP1 modulates activation of B-Raf. Proc Natl Acad Sci USA 104, 10465–10469.
Reshetnikova G, Barkan R, Popov B, Nikolsky N, Chang LS (2000). Disruption of the actin cytoskeleton leads to inhibition of mitogen-induced cyclin E expression, Cdk2 phosphorylation, and nuclear accumulation of the retinoblastoma protein-related p107 protein. Exp Cell Res 259, 35–53.
Roberts PJ, Der CJ (2007). Targeting the Raf-MEK-ERK mitogen-activated protein kinase cascade for the treatment of cancer. Oncogene 26, 3291–3310.
Roskoski R Jr (2012). ERK1/2 MAP kinases: structure, function, and regulation. Pharmacol Res 66, 105–143.
Saba-El-Leil MK, Vella FD, Vernay B, Voisin L, Chen L, Labrecque N, Ang SL, Meloche S (2003). An essential function of the mitogen-activated protein kinase Erk2 in mouse trophoblast development. EMBO Rep 4, 964–968.
Schevzov G, Fath T, Vrhovski B, Vlahovich N, Rajan S, Hook J, Joya JE, Lemckert F, Puttur F, Lin JJ, *et al.* (2008). Divergent regulation of the sarcomere and the cytoskeleton. J Biol Chem 283, 275–283.
Schevzov G, Lloyd C, Gunning P (1992). High level expression of transfected beta-and gamma-actin genes differentially impacts on myoblast cytoarchitecture. J Cell Biol 117, 775–785.
Schevzov G, Lloyd C, Hailstones D, Gunning P (1993). Differential regulation of tropomyosin isoform organisation and gene expression in response to altered actin gene expression. J Cell Biol 121, 811–821.
Schevzov G, Vrhovski B, Bryce NS, Elmir S, Qiu MR, O'Neill GM, Yang N, Verrills NM, Kavallaris M, Gunning PW (2005). Tissue-specific tropomyosin isoform composition. J Histochem Cytochem 53, 557–570.
Schevzov G, Whittaker SP, Fath T, Lin JJ, Gunning PW (2011). Tropomyosin isoforms and reagents. Bioarchitecture 1, 135–164.
Schrick C, Fischer A, Srivastava DP, Tronson NC, Penzes P, Radulovic J (2007). N-cadherin regulates cytoskeletally associated IQGAP1/ERK signaling and memory formation. Neuron 55, 786–798.
Schwartz MA, Assoian RK (2001). Integrins and cell proliferation: regulation of cyclin-dependent kinases via cytoplasmic signaling pathways. J Cell Sci 114, 2553–2560.
Seger R, Krebs EG (1995). The MAPK signaling cascade. FASEB J 9, 726–735.
Skau CT, Neidt EM, Kovar DR (2009). Role of tropomyosin in formin-mediated contractile ring assembly in fission yeast. Mol Biol Cell 20, 2160–2173.
Smith ER, Smedberg JL, Rula ME, Xu XX (2004). Regulation of Ras-MAPK pathway mitogenic activity by restricting nuclear entry of activated MAPK in endoderm differentiation of embryonic carcinoma and stem cells. J Cell Biol 164, 689–699.
Soderberg O, Gullberg M, Jarvius M, Ridderstrale K, Leuchowius KJ, Jarvius J, Wester K, Hydbring P, Bahram F, Larsson LG, *et al.* (2006). Direct observation of individual endogenous protein complexes in situ by proximity ligation. Nat Methods 3, 995–1000.
Stehn JR, Haass NK, Bonello T, Desouza M, Kottyan G, Treutlein H, Zeng J, Nascimento PR, Sequeira VB, Butler TL, *et al.* (2013). A novel class of anticancer compounds targets the actin cytoskeleton in tumor cells. Cancer Res 73, 5169–5182.
Stehn JR, Schevzov G, O'Neill GM, Gunning PW (2006). Specialisation of the tropomyosin composition of actin filaments provides new potential targets for chemotherapy. Curr Cancer Drug Targets 6, 245–256.
Sung LA, Gao KM, Yee LJ, Temm-Grove CJ, Helfman DM, Lin JJ, Mehrpouryan M (2000). Tropomyosin isoform 5b is expressed in human erythrocytes: implications of tropomodulin-TM5 or tropomodulin-TM5b complexes in the protofilament and hexagonal organization of membrane skeletons. Blood 95, 1473–1480.
Tobacman LS (2008). Cooperative binding of tropomyosin to actin. Adv Exp Med Biol 644, 85–94.
Vetterkind S, Poythress RH, Lin QQ, Morgan KG (2013). Hierarchical scaffolding of an ERK1/2 activation pathway. Cell Commun Signal 11, 65.
Villanueva J, Vultur A, Lee JT, Somasundaram R, Fukunaga-Kalabis M, Cipolla AK, Wubbenhorst B, Xu X, Gimotty PA, Kee D, *et al.* (2010). Acquired resistance to BRAF inhibitors mediated by a RAF kinase switch in melanoma can be overcome by cotargeting MEK and IGF-1R/PI3K. Cancer Cell 18, 683–695.
Vlahovich N, Kee AJ, Van der Poel C, Kettle E, Hernandez-Deviez D, Lucas C, Lynch GS, Parton RG, Gunning PW, Hardeman EC (2009). Cytoskeletal tropomyosin Tm5NM1 is required for normal excitation-contraction coupling in skeletal muscle. Mol Biol Cell 20, 400–409.

Voisin L, Saba-El-Leil MK, Julien C, Fremin C, Meloche S (2010). Genetic demonstration of a redundant role of extracellular signal-regulated kinase 1 (ERK1) and ERK2 mitogen-activated protein kinases in promoting fibroblast proliferation. Mol Cell Biol 30, 2918–2932.

Weber JD, Raben DM, Phillips PJ, Baldassare JJ (1997). Sustained activation of extracellular-signal-regulated kinase 1 (ERK1) is required for the continued expression of cyclin D1 in G1 phase. Biochem J 326, 61–68.

Wee S, Jagani Z, Xiang KX, Loo A, Dorsch M, Yao YM, Sellers WR, Lengauer C, Stegmeier F (2009). PI3K pathway activation mediates resistance to MEK inhibitors in KRAS mutant cancers. Cancer Res 69, 4286–4293.

Welsh CF, Roovers K, Villanueva J, Liu Y, Schwartz MA, Assoian RK (2001). Timing of cyclin D1 expression within G1 phase is controlled by Rho. Nat Cell Biol 3, 950–957.

White CD, Brown MD, Sacks DB (2009). IQGAPs in cancer: a family of scaffold proteins underlying tumorigenesis. FEBS Lett 583, 1817–1824.

Yao Y, Li W, Wu J, Germann UA, Su MS, Kuida K, Boucher DM (2003). Extracellular signal-regulated kinase 2 is necessary for mesoderm differentiation. Proc Natl Acad Sci USA 100, 12759–12764.

Yoon S, Seger R (2006). The extracellular signal-regulated kinase: multiple substrates regulate diverse cellular functions. Growth Factors 24, 21–44.